

MARTIN MARIETTA

# Martin Marietta Laboratories

AD-A171 655

MML TR 84-19c

PROTECTION OF ALUMINUM AGAINST  
CORROSION BY INCORPORATION OF  
ORGANIC INHIBITORS INTO PAINTS  
AND PRIMERS

Preliminary  
End-of-First-Year  
Final Technical Report  
July 1984

APPROVED FOR PUBLIC RELEASE:  
DISTRIBUTION UNLIMITED

Prepared for:

Department of the Navy  
Naval Air Development Center

Contract No. N00019-82-C-0439

Prepared by:

G.D. Davis,  
D.K. Shaffer, and  
L.J. Matienzo

Martin Marietta Laboratories  
1450 South Rolling Road  
Baltimore, Maryland 21227

86 9 15 172

AD-A171 655

DTIC ACCESSION NUMBER

PHOTOGRAPH THIS SHEET

MML TR 84-19c

1

LEVEL

PROTECTION OF ALUMINUM AGAINST  
CORROSION BY INCORPORATION OF  
ORGANIC INHIBITORS INTO PAINTS  
AND PRIMERS

INVENTORY

PRELIMINARY END-OF-FIRST-YEAR  
FINAL TECHNICAL REPORT

JULY 84

DOCUMENT IDENTIFICATION

**DISTRIBUTION STATEMENT A**

Approved for public release;  
Distribution Unlimited

DISTRIBUTION STATEMENT

ACCESSION FOR

NTIS GRA&I



DTIC TAB



UNANNOUNCED



DISSEMINATION



BY

DISTRIBUTION

AVAILABILITY CODES

DISC

AVAIL AND OR SPECIAL

A-1

DISTRIBUTION STAMP

DTIC  
ELECTE

SEP 16 1986

D

DATE ACCESSIONED

DATE RETURNED

86 9 15 172

DATE RECEIVED IN DTIC

REGISTERED OR CERTIFIED NO.

PHOTOGRAPH THIS SHEET AND RETURN TO DTIC-DDAC

REPORT DOCUMENTATION PAGE		READ INSTRUCTIONS BEFORE COMPLETING FORM
1. REPORT NUMBER MML TR 84-19c	2. GOVT ACCESSION NO.	3. RECIPIENT'S CATALOG NUMBER
4. TITLE (and Subtitle) Protection of Aluminum Against Corrosion by Incorporation of Organic Inhibitors into paints and primers.		5. TYPE OF REPORT & PERIOD COVERED End-of-First-Year Final Technical Report
		6. PERFORMING ORG. REPORT NUMBER MML TR 84-19c
7. AUTHOR(s) G.D. Davis, D.K. Shaffer and L.J. Matienzo		8. CONTRACT OR GRANT NUMBER(s) N00019-82-C-0439
9. PERFORMING ORGANIZATION NAME AND ADDRESS Martin Marietta Corporation Martin Marietta Laboratories 1450 S. Rolling Road, Balto., MD 21227		10. PROGRAM ELEMENT, PROJECT, TASK AREA & WORK UNIT NUMBERS
11. CONTROLLING OFFICE NAME AND ADDRESS Department of the Navy Naval Air Systems Command Washington, DC 20361		12. REPORT DATE July 1984
		13. NUMBER OF PAGES
14. MONITORING AGENCY NAME & ADDRESS (if different from Controlling Office) Naval Air Development Center Warminster, PA 18974		15. SECURITY CLASS. (of this report) Unclassified
		15a. DECLASSIFICATION/DOWNGRADING SCHEDULE
16. DISTRIBUTION STATEMENT (of this Report)  Approved for public release; distribution unlimited.		
17. DISTRIBUTION STATEMENT (of abstract entered in Block 20, if different from Report)  N.A.		
18. SUPPLEMENTARY NOTES  None		
19. KEY WORDS (Continue on reverse side if necessary and identify by block number)  Corrosion, aluminum, corrosion inhibitors, paints, primers, adhesive bonding.		
20. ABSTRACT (Continue on reverse side if necessary and identify by block number)  Selected organic compounds have been evaluated on the basis of their ability to inhibit corrosion of aluminum and their bonding compatibility with a specified metal-adhesive system. Organic amino phosphonate and silane inhibitors were applied to sulfuric acid-anodized (SAA) 7075-T6 aluminum either		

by direct adsorption from aqueous solution or by spraying an inhibitor-containing primer formulation. All specimens, including the SAA control, exhibited superior corrosion resistance properties with respect to a standard Forest Products Laboratory (FPL) etch treatment. Wedge test adhesion analysis allowed evaluation of the compatibility of inhibitor-treated specimens with an epoxy adhesive (FM-123-2) to simulate the final paint system. The results showed that low concentrations (2-100 ppm) of nitrilotris methylene phosphonic acid (NTMP) forced crack propagation to occur cohesively in the adhesive -- the optimum performance for a given adhesive-adherend system. Phenylphosphonic acid (PPA) and two silane inhibitors (an aminosilane, A-0800, and an epoxysilane, Z-6040) also strengthened the oxide-polymer interface.

In addition to these studies, the SAA oxide was characterized by XPS and XSEM, a mechanism of hydration was proposed, the optimum adsorption conditions (e.g. 30 min, 100 ppm, pH > 3.5 for monolayer NTMP coverage) were determined for the inhibitor compounds, and the kinetic behavior of the epoxy curing reaction was monitored by DSC and FT-IR. An alternative, nonanodizing etch surface preparation has been chosen to efficiently test a wide range of phosphonate, sulfonate and silane inhibitors, prior to their ultimate evaluation for long-term corrosion resistance.

PROTECTION OF ALUMINUM AGAINST CORROSION BY INCORPORATION OF  
ORGANIC INHIBITORS INTO PAINTS AND PRIMERS

G.D. Davis, D.K. Shaffer, and L.J. Matienzo  
Martin Marietta Laboratories  
1450 South Rolling Road  
Baltimore, Maryland 21227

A-1

## TABLE OF CONTENTS

	<u>Page</u>
List of Tables	v
List of Figures	vi
I. INTRODUCTION	1
II. EXPERIMENTAL	3
A. SAMPLE PREPARATION	3
1. Sulfuric Acid Anodized Process	3
2. Chromate Conversion Coating (CCC) Process	3
3. Hydration	3
4. Adsorption	4
5. Epoxy Primer	4
6. Corrosion Testing	4
B. TEST MEASUREMENTS	7
1. Scanning Electron Microscopy	7
2. X-ray Photoelectron Spectroscopy	7
3. Auger Electron Spectroscopy	8
4. Fourier Transform-Infrared Spectrometry	8
5. Differential Scanning Calorimetry	8
6. Salt-Fog Corrosion Test	8
7. Wedge Tests	10
III. RESULTS	11
A. OXIDE CHARACTERIZATION	11
1. Untreated Specimens	11
a. Morphology	11
b. Chemistry	17
2. Hydrated Oxide	17
a. Morphology	17
b. Chemistry	21
B. INHIBITOR ADSORPTION	24
1. NTMP	24
a. Concentration	24
b. pH	27
2. Other Inhibitors	33
C. PRIMER CHARACTERIZATION	33
1. FT-IR Analysis	33
2. DSC Analysis	33
3. Inhibitor Addition to Primer	41
D. CORROSION TESTING	44
1. Salt-Fog Test	44
2. Wedge Test	49

TABLE OF CONTENTS (Continued)

	<u>Page</u>
IV. DISCUSSION	55
A. FRESH SAA OXIDE	55
B. HYDRATION	56
C. ADSORPTION	57
D. INHIBITOR INCORPORATION INTO PRIMER	59
E. CORROSION TESTING	60
1. Salt-Fog Tests	60
2. Wedge Tests	61
VI. CONCLUSIONS AND RECOMMENDATIONS	63
VII. REFERENCES	65

## LIST OF TABLES

	<u>Page</u>
Table 1. Adsorption Solution Concentrations	6
Table 2. XPS Sensitivity Factors (Mg K $\alpha$ Excitation	9
Table 3. Oxide Thickness Measured by XSEM as a Function of Anodization Time	16
Table 4. XPS Surface Composition of 7075-T6 Aluminum as a Function of SAA Anodization Time	18
Table 5. Reported Acidity Constants for Nitrilotris Methylene Phosphonic Acid (NTMP)	29
Table 6. Corrosion Salt-Fog Results on 7075-T6 Test Panels Inhibitor Adsorption	43
Table 7. Corrosion Salt-Fog Results for NADC Chromate Conversion Coated (CCC) Specimens by ASTM 2197-B Rating System	48
Table 8. XPS Analysis of Adjoining Side of Wedge Test Panels	52



## LIST OF FIGURES

	<u>Page</u>
Figure 1. Corrosion inhibitor compounds adsorbed onto 7075-T6 Al SAA surfaces.	5
Figure 2. XSEM micrographs of 7075-T6 SAA oxide surface showing "cracked-mud" morphology.	12
Figure 3. XSEM stereo micrographs of 7075-T6 SAA oxide surface showing porosity.	13
Figure 4. XSEM cross-sectional micrographs of 7075-T6 SAA oxide layer.	14
Figure 5. Isometric drawing of SAA oxide morphology, including dimensions for the oxide depth, the width of the crevices between cellular bundles, and individual cell and pore diameters.	15
Figure 6. XSEM micrographs of 7075-T6 SAA oxide surface after immersion in 80°C water for 10 min.	19
Figure 7. XSEM micrographs of 7075-T6 SAA oxide surface after immersion in 80°C water for 30 min.	20
Figure 8. XPS survey scans for SAA Al coupons immersed in water at 80°C for (a) zero min and (b) 30 min.	22
Figure 9. $Al_2O_3 - Al_2(SO_4)_3 - H_2O$ surface behavior diagram showing the evolution of the surface composition of SAA-treated Al surfaces immersed in 80°C water, as a function of immersion time. The different symbols represent different experimental runs and the numbers represent exposure time in minutes.	23
Figure 10. Adsorption of inhibitor onto SAA oxide surface: P/Al atomic ratio vs time of immersion (min) in 100-ppm NTMP solution.	25

## LIST OF FIGURES (CONTINUED)

	<u>Page</u>
Figure 11. Adsorption of inhibitor onto SAA oxide surface: P/Al atomic ratio vs NTMP concentration over a 0.1- to 10,000-ppm range.	26
Figure 12. The relationship of pH vs NTMP concentration over a 0.1 to 10,000-ppm range, including acidity constant values.	28
Figure 13. The relationship of the P/Al atomic ratio vs pH for a 100 ppm NTMP solution over a pH range of 1.5 to 11., Acidity constant values are also shown.	30
Figure 14. Deprotonation (dissociation) reactions for nitrolotris methylene phosphonic acid (NTMP).	31
Figure 15. Adsorption of phosphonate and silane inhibitors onto SAA oxide surface.	32
Figure 16. FT-IR spectrum of EPON 1001-T75 epoxide resin.	34
Figure 17. FT-IR spectrum of Versamid 115 polyamide resin.	35
Figure 18. FT-IR kinetics plot of epoxide band ( $917\text{ cm}^{-1}$ ) during epoxy-polyamide curing reaction at $50^{\circ}\text{C}$ .	36
Figure 19. Kinetics plot of FT-IR analysis of epoxy-polyamide curing reaction.	37
Figure 20. DSC kinetics plot of epoxy-polyamide curing reaction.	38
Figure 21. Correlation of FT-IR (--) and DSC (--) kinetics data for epoxy curing reaction.	39
Figure 22. DSC thermal transition curve for epoxy-curing reaction.	40

## LIST OF FIGURES (CONTINUED)

	<u>Page</u>
Figure 23. DSC thermal transition curves for inhibitor, solvent and epoxy system: (a) NTMP, (b) B component only, (c) B + iPrOH, (d) B + iPrOH + NTMP, (e) A + B, (f) A + B + iPrOH, (g) A + B + iPrOH + NTMP, and (h) A + B + NTMP mull. The 160- 180°C range is indicated by cross-hatching on each scale.	42
Figure 24. Photographs of Martin Marietta Laboratories test panel: SAA treated with NTMP (5000 ppm) (a) before and (b) after exposure in salt-fog chamber (1250 hr).	45
Figure 25. Photographs of Martin Marietta Laboratories test panel: CCC treated with NTMP (5000 ppm) (a) before and (b) after exposure in salt-fog chamber (1250 hr).	46
Figure 26. Photographs of duplicate NADC test panels: CCC treated with NTMP (5000 ppm) after exposure in salt-fog chamber (1000 hr).	47
Figure 27. Crack length vs time curve for wedge tests using various specimen treatments.	50
Figure 28. Crack length vs time curve for wedge test using various specimen treatment.	51

## I. INTRODUCTION

The protection of aluminum against corrosion by organic compounds that are compatible with adhesively bonded paint systems has important applications for the aircraft industry. Proper pretreatment of the aluminum prior to epoxy bonding remains essential for developing high bond strengths.<sup>(1-6)</sup> However, the additional incentive to eliminate environmentally undesirable materials, such as chromates, has led to the consideration of organic inhibitor compounds.

In previous investigations, the importance of the microscopic morphology of the oxide surface for good bondability of Al adherends has been demonstrated.<sup>(7-12)</sup> Because surface roughness controls the degree of mechanical interlocking with the overlying polymer (for systems in which the chain length increases upon curing), it is regarded as the single most important factor in determining both initial bond strength and long-term bond durability.

A second critical requirement for long-term durability of aluminum-polymer bonds is the stability of the aluminum oxide in a humid environment.<sup>(6,12-15)</sup> The ultimate hydration of the oxide to the oxyhydroxide severely degrades the overall bond strength as the result of a volume expansion and morphology change that induce stress at the polymer-hydroxide interface and result in poor adherence to the base Al.

The use of hydration inhibitors to improve bond durability of Al adhesive joints, by inhibiting the oxide-to-hydroxide conversion process, has been demonstrated with certain organic amino phosphonate compounds.<sup>(16-19)</sup> In particular, nitrilotris methylene phosphonic acid (NTMP) has been shown to improve the durability of treated Forest Products Laboratories (FPL) and

phosphoric acid anodized (PAA) bonded structures relative to their untreated analogs. More recently, specific characteristics that promote good bond performance have been identified for NTMP and related inhibitor compounds, including coupling of the oxide to the adhesive or primer.<sup>(19)</sup>

A more widespread example of adhesive bonding to metals and alloys involves painted coatings, the most common method for combating corrosion. These coatings, like adhesives, must be properly applied to a suitably prepared surface. Thus, a process that combines adequate substrate pretreatment and the incorporation of effective organic corrosion inhibitors, which can maintain or improve the adhesion of the applied paint coating, should provide an overall superior protective system for the metal as well as help to reduce or eliminate the use of hazardous compounds.

Accordingly, we have conducted investigations in the following four areas: (1) Characterization of the sulfuric acid anodized (SAA) oxide surfaces using high-resolution scanning electron microscopy (XSEM) and X-ray photoelectron spectroscopy (XPS); (2) screening of selected inhibitor compounds for their adsorption properties, with subsequent analysis by the same (XPS, XSEM) surface techniques; (3) characterization of the curing reaction of the primer system and analysis of the effects of added inhibitor compounds on this process, using Fourier Transform-Infrared Analysis (FT-IR) and differential scanning calorimetry (DSC); and (4) evaluation of the anticorrosion and adhesive compatibility of the adsorbed inhibitor and inhibitor-containing primer systems using the salt fog procedure (ASTM B-117) and wedge test (ASTM D-3762), respectively.

## II. EXPERIMENTAL

### A. SAMPLE PREPARATION

#### 1. Sulfuric Acid Anodized Process.

All 7075-T6 test coupons (1 cm x 1 cm or 2.5 cm x 7.6 cm) and corrosion test panels were degreased with trichloroethylene, washed with TURCO 4215-S alkaline solution, and rinsed in distilled water. The coupons were anodized in a 10% sulfuric acid solution (v:v) at 25°C and 15 volts for the time specified, rinsed in deionized distilled water,\* and dried by forced ambient air.

#### 2. Chromate Conversion Coating (CCC) Process.

A standard chromate conversion coating (Iridite)\*\* was applied to nonanodized 7075-T6 specimens at the Naval Air Development Center (NADC) following pretreatment cleaning procedures. The panels were then air dried prior to corrosion (salt fog) testing.

#### 3. Hydration.

SAA surfaces were hydrated by immersing freshly treated coupons in deionized distilled water held at 80°C. Samples were removed at intervals ranging from 1 minute to 2 hours, dried by forced air, and stored in a dessicator.

---

\* Unless otherwise specified, all aqueous rinsings and immersion solutions following the TURCO bath were conducted with deionized distilled water.

\*\* Iridite 14-2 (Certified to MIL-C-81706).

#### 4. Adsorption.

Several inhibitors were adsorbed onto SAA surfaces during the course of this year's program. These are shown in Figure 1. Adsorption was accomplished by immersing the coupons or panels in an aqueous solution of the desired inhibitor for a specified time (generally 30 or 60 minutes). Solution concentrations, which depended on the measurement or test that followed, are listed in Table I. In most cases, the solutions were unbuffered, allowing the pH to be determined by the inhibitor concentration. However, for one adsorption study, the pH was accordingly adjusted from 1.5 to 11 by adding either  $H_2SO_4$  or NaOH. In all cases, removed specimens were rinsed in fresh, deionized distilled water and dried with forced ambient air.

#### 5. Epoxy Primer.

The epoxy primer system consisted of Component A (Shell EPON 1001-T75 epoxy resin) and Component B (Versamid 115 polyamide curing agent). To study the curing kinetics of the primer by DSC, we combined unpigmented epoxy-polyamide A and B components (neat) in a 1:1 (wt:wt) ratio for analysis by DSC. We also applied a small portion of this mixture to NaCl plates for FT-IR analysis. The plates were heated in a temperature-controlled oven and spectra were taken at appropriate time-intervals until the curing process was completed.

#### 6. Corrosion Testing.

Bare 7075-T6 test panels were prepared by SAA and chromate conversion coating methods as previously described. Panels to be treated with NTMP or A-0800 were immersed in a 0.5% (v:v) solution of inhibitor (a standard concentration used for silane couplers as adhesion promoters), in 1:1 methanol: water,

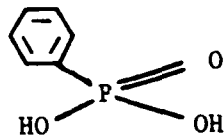
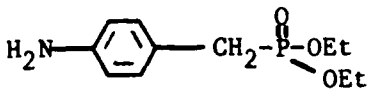
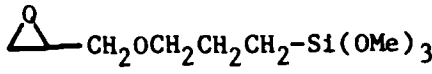
<u>Designation</u>	<u>Chemical Name</u>	<u>Structure</u>
NTMP	Nitrilotris methylene phosphonic acid	$\text{N} - \left( \text{CH}_2 - \text{P} \begin{array}{c} \text{O} \\ \parallel \\ \text{OH} \end{array} \right)_3$
PPA	Phenylphosphonic acid	
DABP	Diethyl p-aminobenzylphosphonate	
A-0800	$\gamma$ -aminopropyltrimethoxysilane	$\text{H}_2\text{N}-\text{CH}_2\text{CH}_2\text{CH}_2-\text{Si}(\text{OMe})_3$
Z-6040	( $\gamma$ -glycidoxypropyl) trimethoxysilane	

Figure 1. Corrosion inhibitor compounds adsorbed onto 7075-T6 Al SAA surfaces.



Table I  
Adsorption Solution Concentrations

<u>Inhibitor</u> <sup>a</sup>	<u>Concentration (ppm)</u>		
	<u>XPS</u>	<u>Experiment Salt Fog</u>	<u>Wedge Test</u>
NTMP	0.1-10,000	5000	2-5000
PPA	0.3-100	5000	100-500
DABP	0.3-100	5000	- - - -
Z-6040	1-10,000	---	200-5000
A-0800	-----	5000	500

<sup>a</sup> See Figure 1 for identification.

rinsed and then sprayed with the primer to a thickness of 0.015 - 0.023 cm. Other panels were sprayed with primer in which either DABP or PPA had been dissolved in the B component. The panels were then scribed and the cut edges were sealed according to ASTM D-1654, prior to corrosion-chamber exposure.

## B. TEST MEASUREMENTS

### 1. Scanning Electron Microscopy.

Test specimens were cut, mounted, and sputter-coated with a thin layer of platinum to provide electrical conductivity over the entire morphological surface. The samples were then examined by SEM in a JEOL JEM-100CX scanning transmission electron microscope (STEM), which provided magnifications of 10-50,000X at a resolution of 30 Å (XSEM). Cross-sectional specimens were fractured, either at room temperature or under liquid nitrogen, prior to mounting orthonormal to the stage for examination.

### 2. X-ray Photoelectron Spectroscopy.

The composition of the treated and untreated surfaces was measured by XPS using a Physical Electronics Model 548 spectrometer, which consists of a double-pass cylindrical mirror analyzer (CMA) with pre-retarding grids and a coaxial electron gun, a Mg K $\alpha$  X-ray source, an ion sputter gun, a gas handling system, and a dedicated minicomputer to facilitate data acquisition and analysis. Survey scans for each sample were obtained using a pass energy of 200eV; for most samples, high-resolution spectra (pass energy of 50eV) were obtained from the O 1s, Al 2p, S 2p, and P 2p photoelectron lines. The atomic composition of

the surface was determined from the area under the photoelectron lines and sensitivity factors were derived from standards measured by this instrument (Table II).

### 3. Auger Electron Spectroscopy.

The XPS analyses were occasionally supplemented by AES combined with ion sputtering to obtain a distribution of elements with depth. An estimate of the depth scale was obtained by sputtering Ta foil, anodized to give a known oxide thickness, combined with earlier measurements, which indicated that  $\text{Al}_2\text{O}_3$  has a sputtering rate of 60% of  $\text{Ta}_2\text{O}_5$ .<sup>(20)</sup>

### 4. Fourier Transform-Infrared Spectrometry.

The curing kinetics of the epoxy-polyamide primer formulation were studied at different temperatures by monitoring the epoxide absorption band at  $917\text{ cm}^{-1}$  as a function of time. A mixture of A and B components (1:1, wt:wt) was placed on NaCl plates and analyzed directly by FT-IR over a spectral range of  $4000\text{--}400\text{ cm}^{-1}$  using a Nicolet 7199 interfaced to a NIC-1180 data acquisition system.

### 5. Differential Scanning Calorimetry.

Equal weights of epoxy A and B components (neat) were combined in the calorimeter micropan, which was subsequently sealed and then placed in a Mettler Instruments DSC-30. The DSC analysis was performed by linearly increasing the temperature from  $-10^\circ$  to  $250^\circ\text{C}$  at a constant rate (e.g.  $10^\circ\text{C}/\text{min}$ ).

### 6. Salt-Fog Corrosion Test.

The prepared specimens were subjected to a specified 5% salt (NaCl) atmosphere in the Labs' Singleton Opti-Mist Test Cabinet. The pH was maintained between 6.5 and 7.2 at a temperature of  $35^\circ\text{C}$ , according to ASTM B-117. The

Table II

XPS Sensitivity Factors (Mg K $\alpha$  Excitation)

<u>Photoelectron Line</u>		<u>Sensitivity Factor</u>
C	1s	0.33
O	1s	1.00
Al	2p	0.20
Si	2p	0.26
P	2p	0.51
S	2p	0.80

specimens, supported on angle-grooved wooden racks in the cabinet, were removed only briefly for periodic inspection during the testing.

#### 7. Wedge Tests.

The corrosion resistance of the treated surfaces was further evaluated by wedge tests (ASTM D-3762). Panels (15 cm x 15 cm) were bonded together using American Cyanamid FM-123-2 epoxy adhesive and cured at 250°F under 40 psi for 1 hr. The panels were then cut into 2.5 cm x 15 cm strips and a wedge (2.5 cm x 2.5 cm x 0.318 cm) was driven in one end. After the induced crack was allowed to equilibrate for one hour, the strips were placed in a humidity chamber at 60°C and 95-100% relative humidity. They were removed at specified times, the location of the crack were marked, and the specimens were returned to the humidity chamber. Following completion of the experiment, some panels were pulled apart and the near-crack tip region was examined by XPS and XSEM to determine the locus of failure.

### III. RESULTS

#### A. OXIDE CHARACTERIZATION

##### 1. Untreated Specimens

###### a. Morphology.

The SAA process forms a thick, porous oxide layer which offers good protection for the base aluminum. The micrographs taken during XSEM analysis (Figures 2 - 4) indicated a "cracked-mud" morphology at low magnifications and a dense porous network at high magnification. An isometric drawing of the SAA oxide morphology shown in Figure 5 illustrates that the porous oxide consists of a thin barrier layer under a dense network of closely-packed pore cells (200-600Å in diameter with the pores 100-300Å wide). The cells generally are oriented in long, columnar bundles, which are separated by relatively wide crevices. Similar descriptions of SAA oxides have also been reported.(12,21-23)

In the cross-sectional SEM analysis, the oxide thickness can be monitored as a function of the anodization time. With the conditions employed (10% H<sub>2</sub>SO<sub>4</sub>, 15V), the oxide grows to > 9.0 µm after a 20-minute anodization. The oxide thicknesses are summarized in Table III.

Ion sputtering of the oxide surfaces while performing Auger analysis yielded depth profiles which also provided a measure of the oxide thickness. However, these thickness values were consistently lower (approximately one-half) than the corresponding values obtained by SEM analysis. This discrepancy reflects the average density of the oxide, in that an AES depth profile provides a measure of the total amount (mass) of oxide removed whereas a SEM micrograph

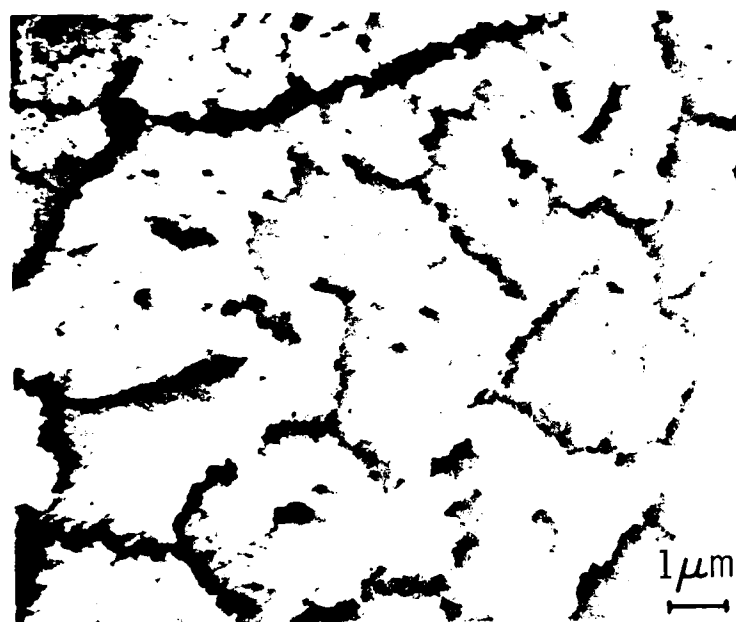
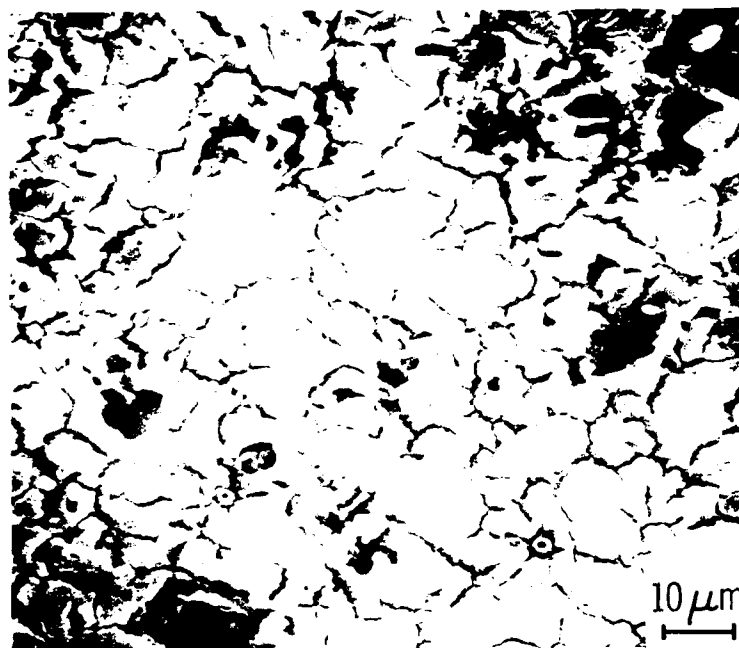


Figure 2. XSEM micrographs of 7075-T6 SAA oxide surface showing "cracked-mud" morphology.

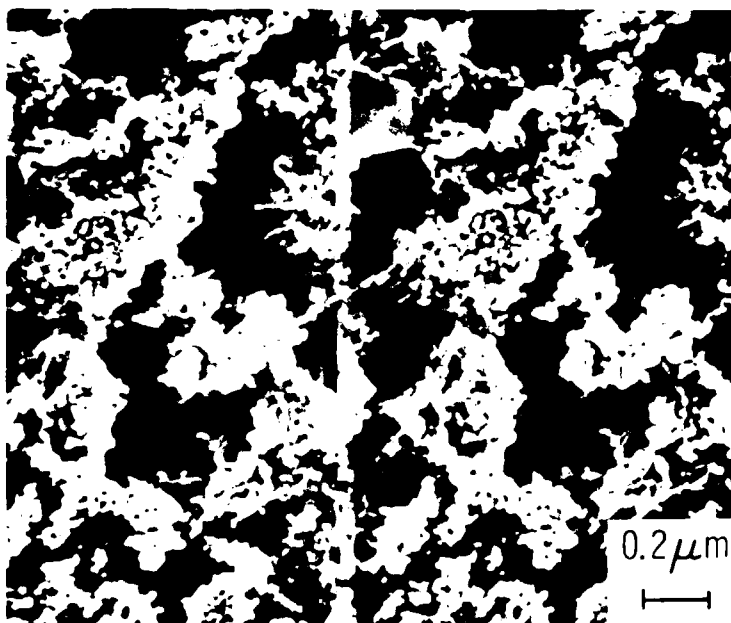
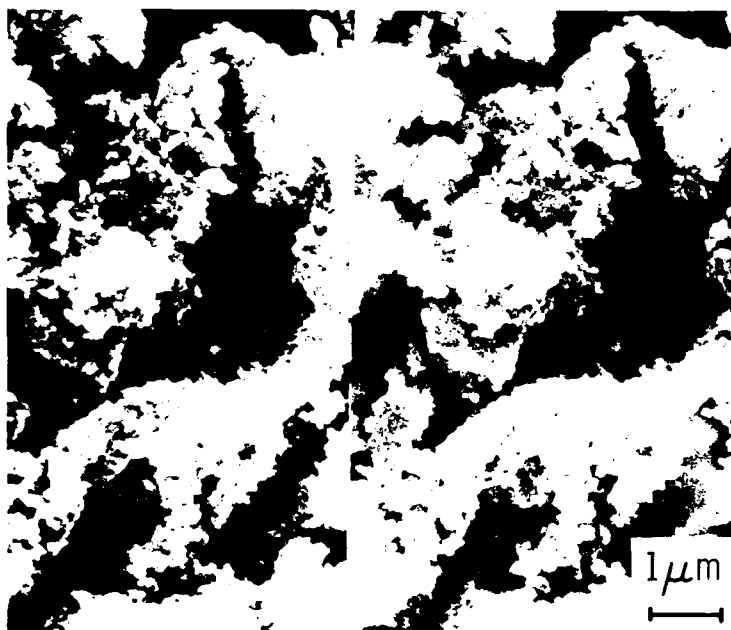


Figure 3. XSEM stereo micrographs of 7075-T6 SAA oxide surface showing porosity.



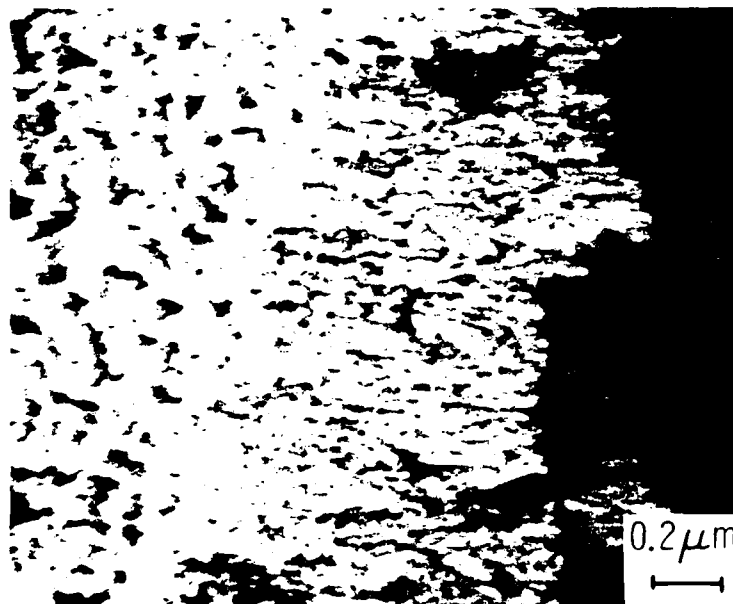


Figure 4. XSEM cross-sectional micrographs of 7075-T6 SAA oxide layer.

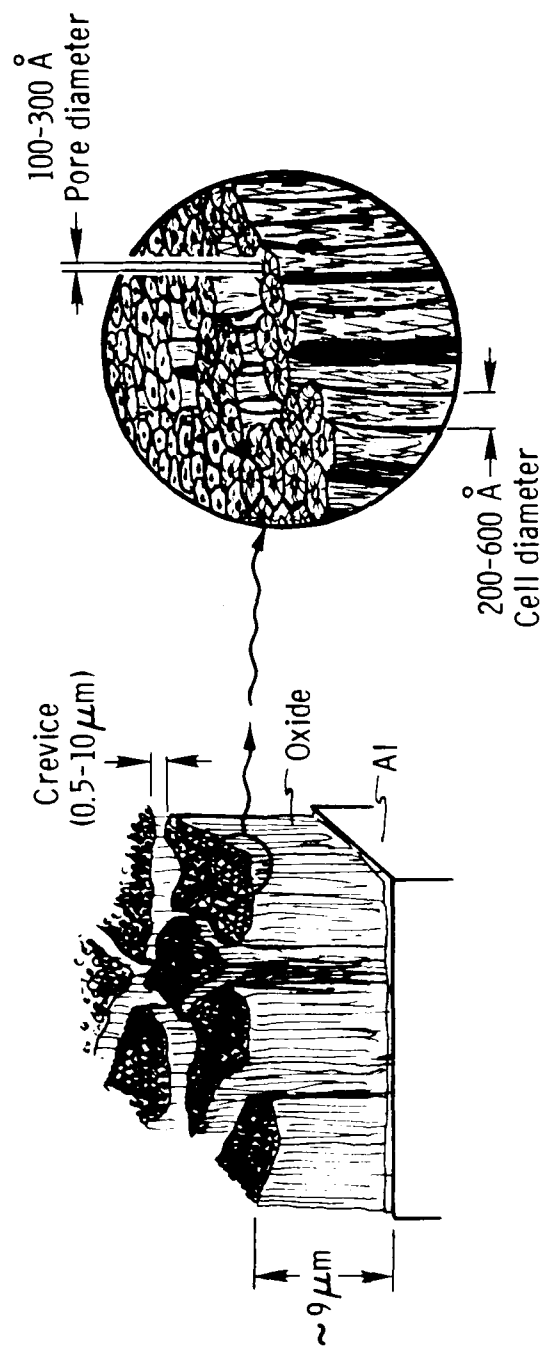


Figure 5. Isometric drawing of SAA oxide morphology, including dimensions for the oxide depth, the width of crevices between cellular bundles, and individual cell and pore diameters.

Table III

Oxide Thickness Measured by XSEM as a  
Function of Anodization\* Time

<u>7075-T6 Treatment</u>	<u>Oxide Thickness (<math>\mu\text{m}</math>)</u>	
	<u>XSEM</u>	<u>AES</u>
Untreated	0	<0.01
SAA: 10 sec	0.15 - 0.20	0.078
30 sec	0.40 - 0.50	0.26
1 min	0.75	---
2 min	1.4	0.78
5 min	1.9 - 3.0	---
10 min	4.5	---
20 min	> 9.0	---

\*Sulfuric acid anodization (SAA, 10%  $\text{H}_2\text{SO}_4$ ) at 15 volts for time indicated.  
For 20 min, the current density decreased from 2.1 to 0.62  $\text{A}/\text{dm}^2$ .

indicates the actual physical dimensions of the oxide.<sup>(24,25)</sup> Consequently, a porous oxide like SAA will appear thinner when measured by AES than when measured by SEM.

b. Chemistry.

The composition of the anodized 7075-T6 surface was analyzed using XPS. The data generally indicated a relatively constant oxide composition after five-minute anodization, i.e., approximately 30% Al, 60% O, 3.5% S and 6.4% C. These values correspond to essentially one monolayer of  $\text{Al}_2(\text{SO}_4)_3$  or  $\text{Al}(\text{HSO}_4)_3$  on top of the  $\text{Al}_2\text{O}_3$ , and little or no  $\text{H}_2\text{O}$ . Adsorbed water was detected in a few cases. It is believed to be weakly bonded, and should be easily removed by heating or by storing under vacuum.<sup>(26-28)</sup> The carbon contribution is believed due to adventitious hydrocarbon contamination originating either from the adsorption solution or from the atmosphere during transfer of the coupons to the spectrometer. The surface composition results are presented in Table IV.

2. Hydrated Oxide.

a. Morphology.

Significant morphological changes accompany the hydration of the SAA surface. After aqueous immersion for 10 minutes (80°C), the deep cracks in the oxide have essentially sealed shut, and a hydrated "corn flake" structure, representative of boehmite ( $\text{Al}(\text{OH})_3$ ),<sup>(11)</sup> is apparent. Immersion for longer times (up to 2 hr) does not cause significant further surface changes. This process is illustrated in the series of micrographs in Figures 6 and 7. A similar hydration process has been observed for several porous aluminum oxide structures.<sup>(11,26,29)</sup>

Table IV  
XPS Surface Composition of 7075-T6 Aluminum as a  
Function of SAA Anodization Time

Specimen Treatment	Elemental Atomic %				S/Al
	Al	O	S	C	
Untreated	6.4	53.5	13.8	26.9	2.2
TURCO only	20.0	41.0	0.5	35.5	0.025
SAA: 0 min.	30.7	45.0	2.1	22.2	0.068
1 min.	30.0	55.1	3.3	11.6	0.11
5 min.	29.4	60.6	3.5	6.4	0.12
10 min.	31.2	59.6	3.7	5.5	0.12
20 min.	29.7	59.7	3.3	7.3	0.11
				P (1.9) Cr (1.1)	

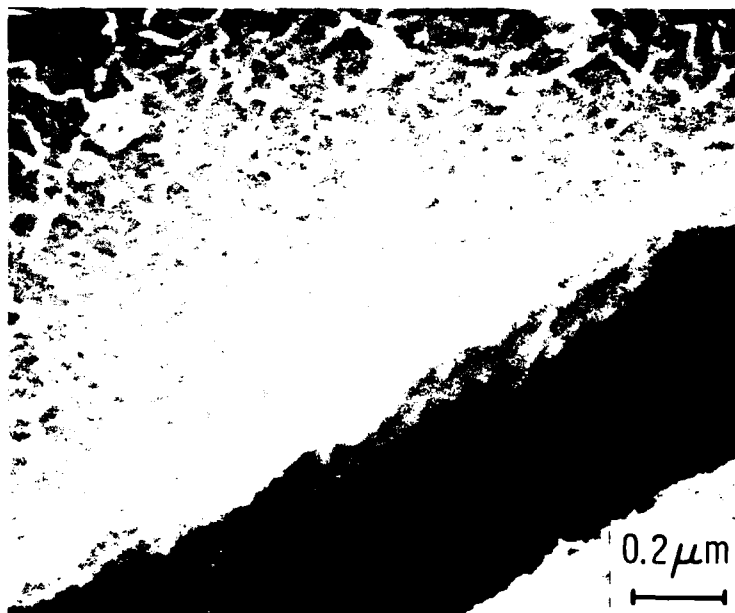
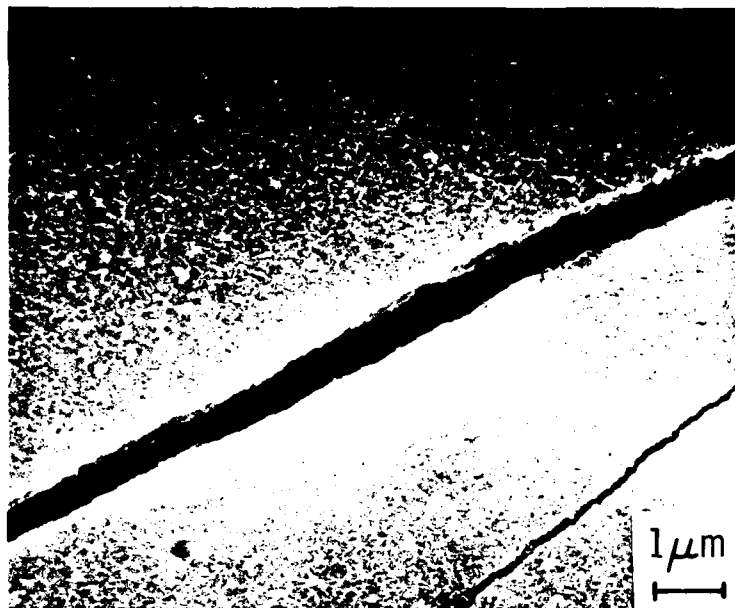


Figure 6. XSEM micrographs of 7075-T6 SAA oxide surface after immersion in 80°C water for 10 min.

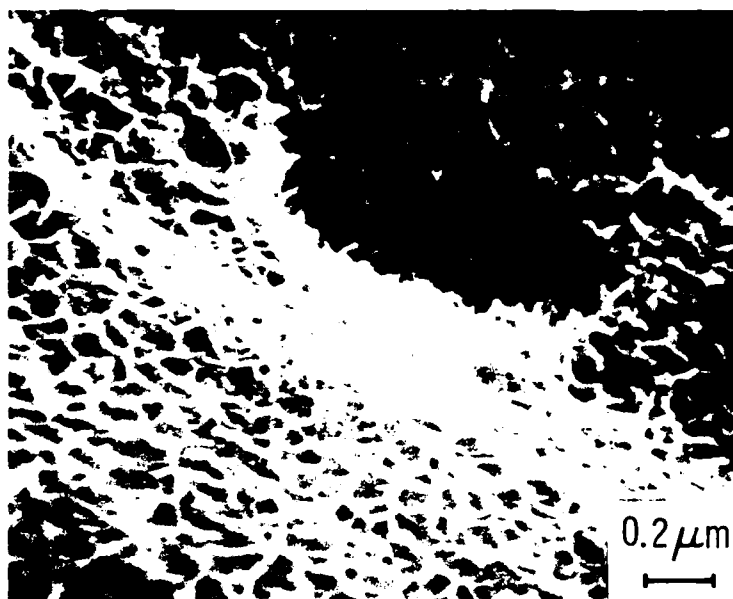
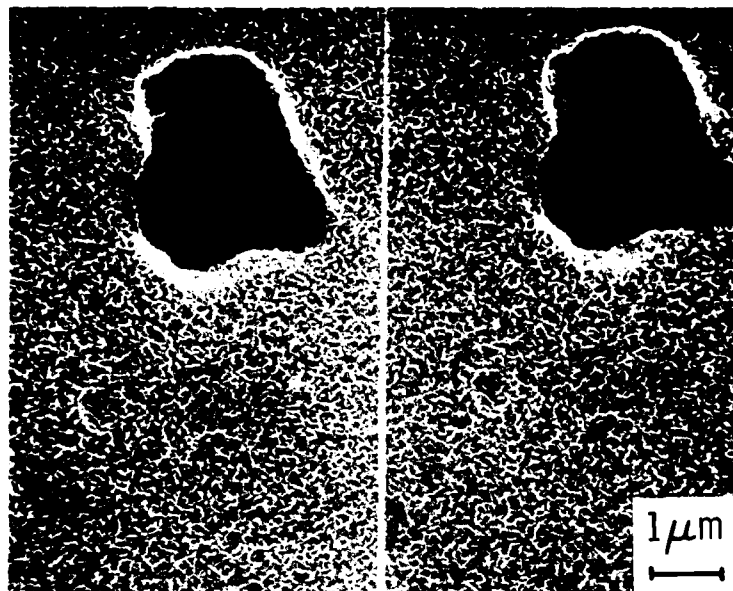


Figure 7. XSEM micrographs of 7075-T6 SAA oxide surface after immersion in 80°C water for 30 min.

b. Chemistry.

The composition of the oxide during hydration was monitored by XPS (Figure 8) and the measurements are very consistent with the XSEM results. To facilitate interpretation of the results, the compositions are displayed on a surface behavior diagram (SBD), a recently developed tool for analysis of surface-sensitive measurements. These diagrams allow the evolution of the surface composition to be traced during hydration. Similar SBD's have previously been invaluable in establishing the steps of the hydration process of phosphoric acid anodized (PAA) aluminum surfaces,<sup>(16,14,26)</sup> determining desired characteristics of hydration inhibitors designed to improve adhesive bond durability,<sup>(19)</sup> and characterizing the interfacial chemistry between (Hg,Cd)Te and its anodic oxide.<sup>(30)</sup> The SBD's, such as the one shown in Figure 9 and described below, resemble ternary phase diagrams, in that they express a composition in terms of three basis compounds. However, they have two important differences: 1) they display surface compositional information instead of bulk structural information, and 2) the equilibrium condition is relaxed so that the evolution of the surface composition can be traced during irreversible reactions, such as the hydration of aluminum.

Figure 9 is an  $\text{Al}_2\text{O}_3 - \text{Al}_2(\text{SO}_4)_3 - \text{H}_2\text{O}$  SBD displaying the composition of SAA surfaces at different stages of hydration. Here the O, Al, and S atomic concentrations determined by XPS have been converted via a linear transformation<sup>(26,30)</sup> to molar concentrations of  $\text{Al}_2\text{O}_3$ ,  $\text{Al}_2(\text{SO}_4)_3$ , and  $\text{H}_2\text{O}$ . The SBD shows the initial surface to be  $\text{Al}_2\text{O}_3$  with the equivalent of approximately one monolayer of sulfate. On some surfaces, some adsorbed water is also present, the amount of which is dependent on the storage conditions.<sup>(19,26)</sup>



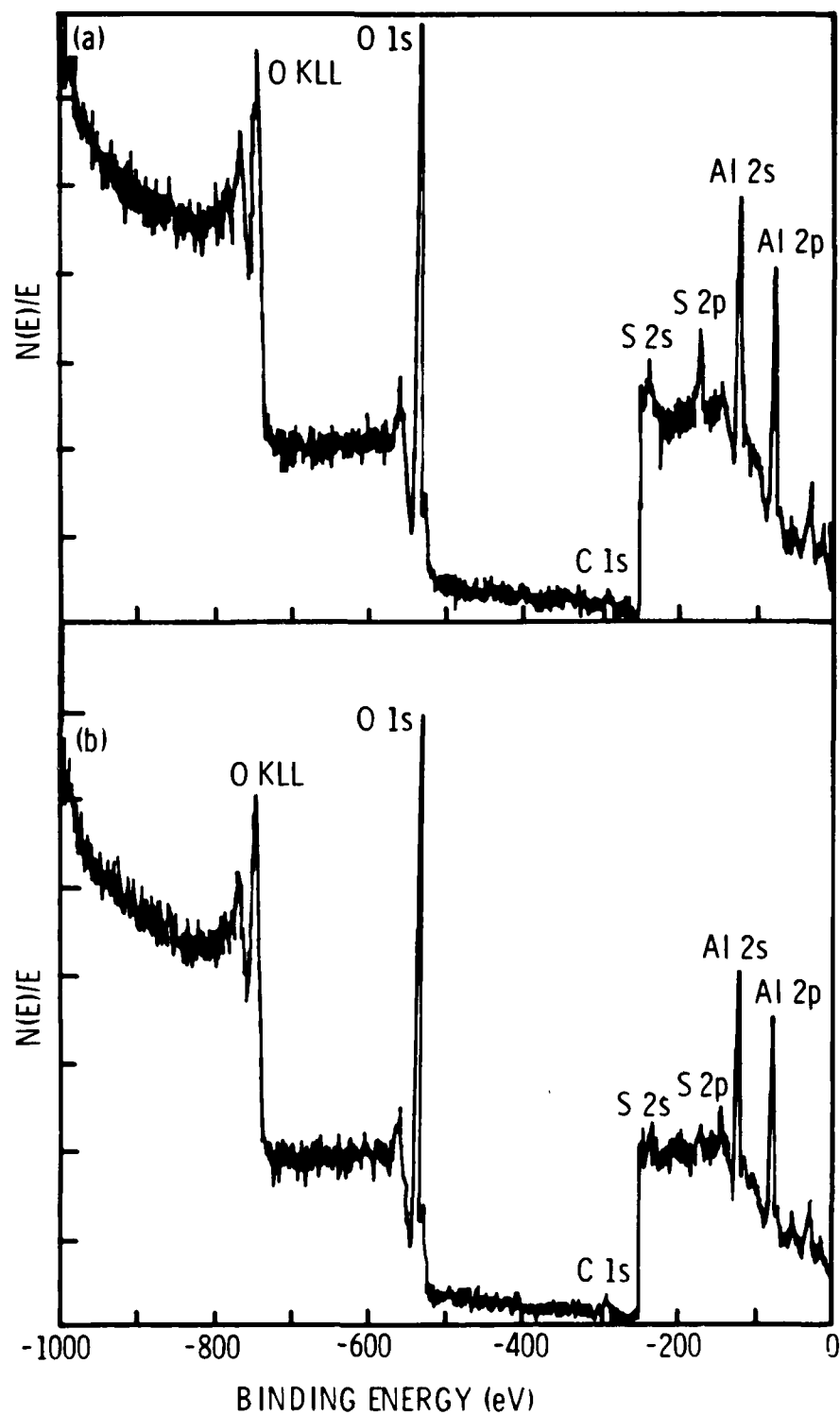


Figure 8. XPS survey scans for SAA Al coupons immersed in water at 80°C for (a) zero min and (b) 30 min.

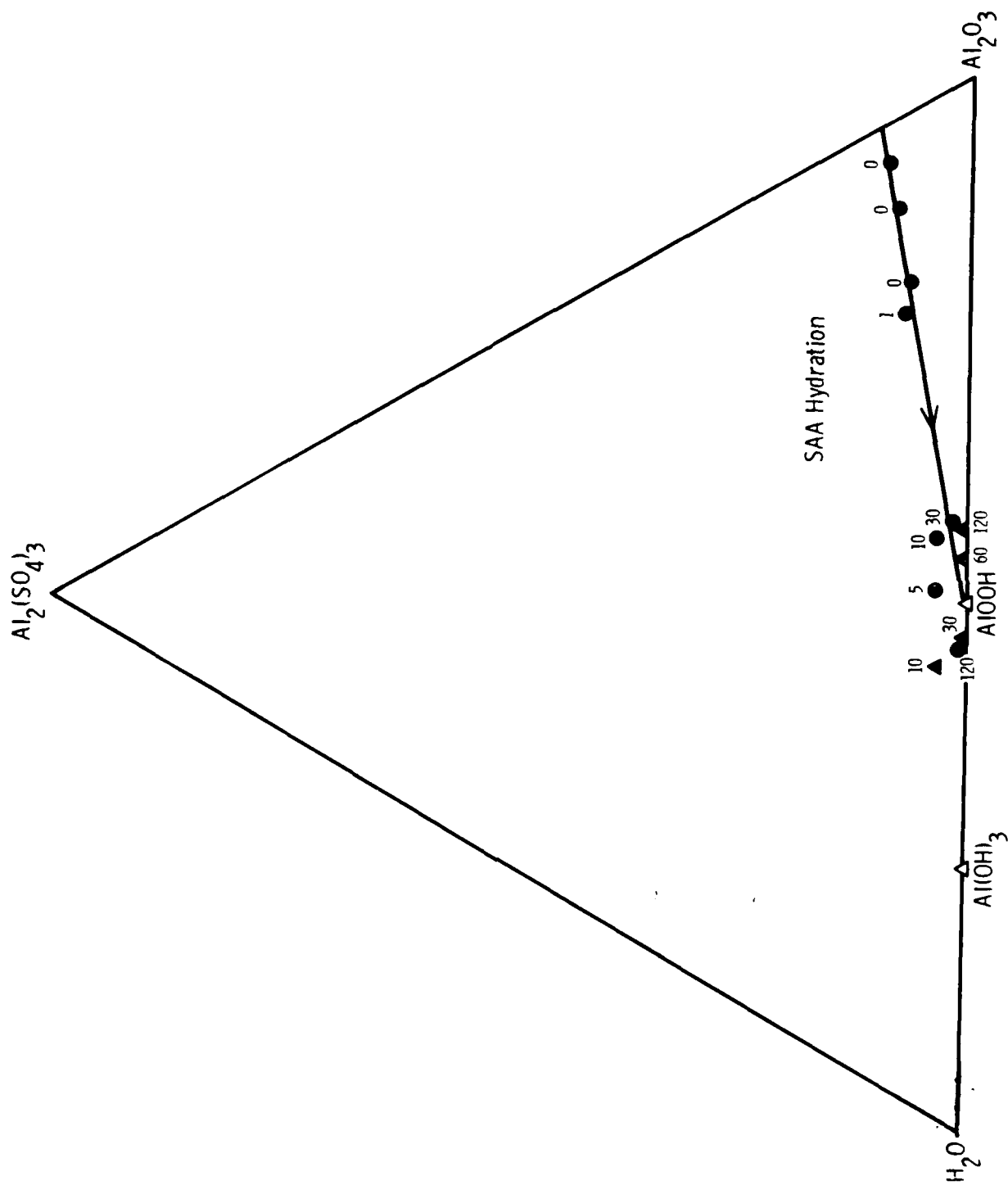


Figure 9. Al<sub>2</sub>O<sub>3</sub> - Al(SO<sub>4</sub>)<sub>3</sub> - H<sub>2</sub>O surface behavior diagram showing the evolution of the surface composition of SAA-treated Al surfaces immersed in 80°C water, as a function of immersion time. The different symbols represent different experimental runs and the number represent exposure time in minutes.

Hot-water immersion for ~ 10 minutes or more causes the surface to hydrate with the consequent growth of boehmite ( $\text{AlOOH}$ ). As shown by the micrographs of Figures 6 and 7, in this process, the porous structure of the oxide is sealed.

## B. INHIBITOR ADSORPTION

### 1. NTMP.

The ability of phosphonate inhibitors to be adsorbed onto a SAA oxide surface can be evaluated by immersing the specimens in a solution of the inhibitor and measuring the subsequent surface concentrations of P and Al by XPS. A plot of P/Al vs immersion time for different inhibitor concentrations indicates the relative adsorption rates and saturation times for the systems. According to Figure 10, which shows this relationship for a 100-ppm NTMP solution, the inhibitor reached saturation by 30 minutes. This time is significantly longer than that required for FPL- and PPA prepared surfaces.<sup>(19)</sup>

#### a. Concentration.

A correlation of phosphorus coverage with inhibitor concentration is shown in Figure 11 for NTMP over a range of  $10^{-1}$  to  $10^4$  ppm and an immersion time of 30 minutes. The graph indicates a P/Al ratio of 0.1 - 0.2, which corresponds to approximately one monolayer coverage of the inhibitor for a FPL surface,<sup>(16)</sup> to occur between 10- and 100-ppm NTMP. Similarly treated FPL surfaces exhibit a much higher resistance to hydration (up to two orders of magnitude) than untreated surfaces. Furthermore, the long-term durability of

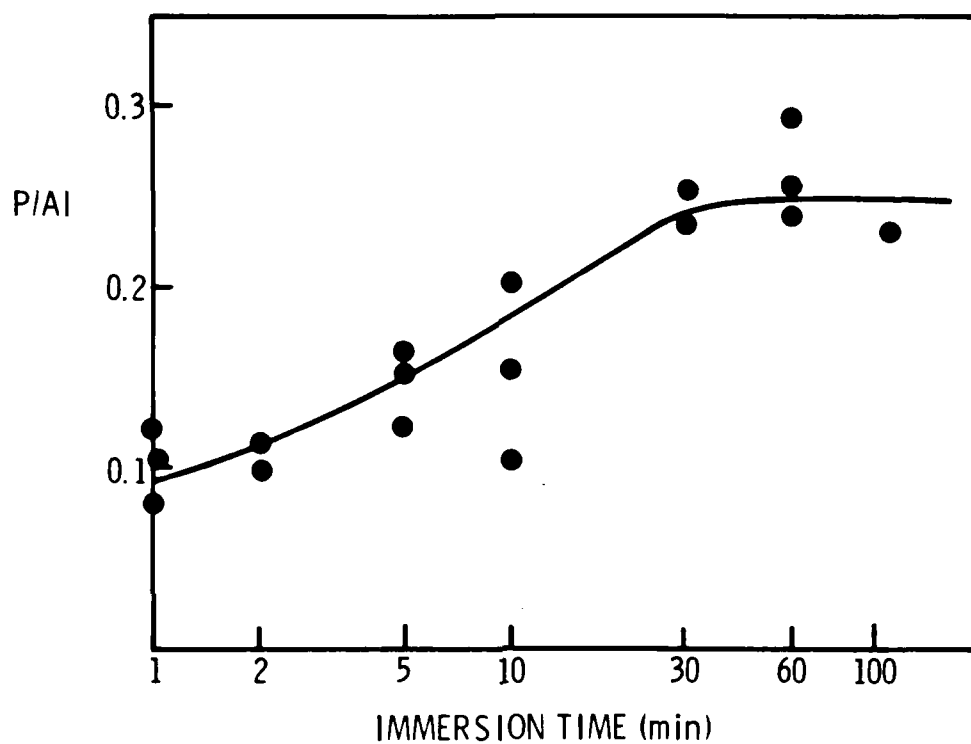


Figure 10. Adsorption of inhibitor onto SAA oxide surface: P/Al atomic ratio vs time of immersion (min) in 100-ppm NTMP solution.

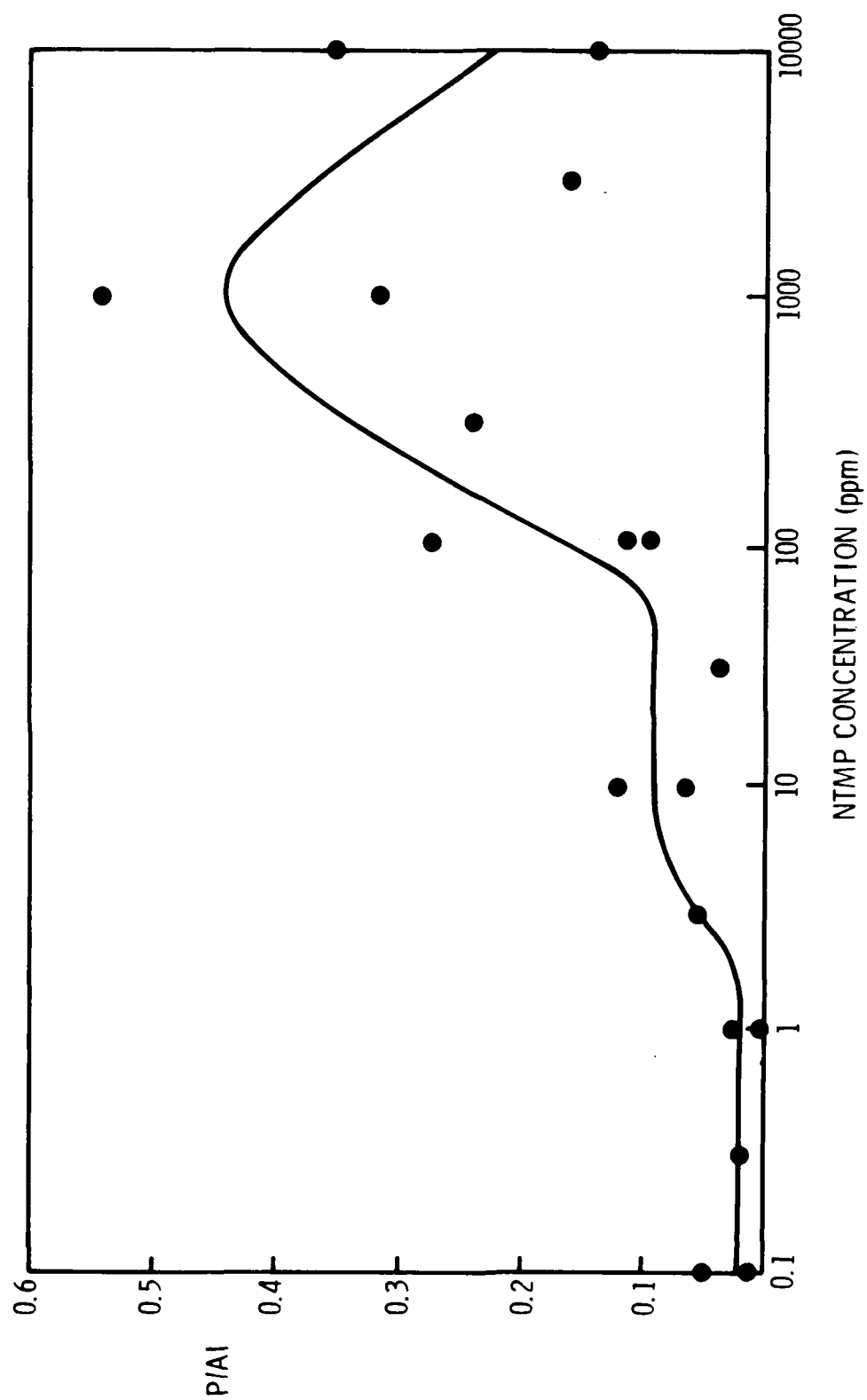


Figure 11. Adsorption of inhibitor onto SAA oxide surface: P/AI atomic ratio vs NTMP concentration over a 0.1- to 10,000-ppm range.

adhesive bonds made with this type of surface is maximized at a monolayer coverage of inhibitor.<sup>(6)</sup>

The data also show that the coverage increases to greater than a monolayer value until it reaches a maximum near 1000 ppm. It then decreases to approximately monolayer coverage after immersion in a 10,000 ppm solution. This multilayer coverage has not been detected before on well-rinsed oxidized aluminum surfaces treated at room temperature.

b. pH.

To determine if changes in the pH of the NTMP solutions were responsible for the adsorption maximum shown in Figure 11, we measured the pH of the solutions as a function of NTMP concentration (Figure 12). The acidity constant ( $pK_a$ ) values shown in this figure were determined by Carter et al.<sup>(31)</sup> These and experimental  $pK_a$  values obtained by other researchers can be compared in Table V. Subsequently, coupons were immersed in 100-ppm solutions with the pH varying from 1.5 to 11. The NTMP surface coverages of these samples are shown in Figure 13. According to the data, adsorption is approximately constant with immersion in solutions of  $pH > 3.5$ . At  $pH \sim 3$ , however, an apparent increase in the coverage is noted, whereas at lower pH, the coverage drops dramatically, so that very little NTMP is adsorbed from solutions of  $pH < 2$ . Such results suggest that the adsorption behavior observed at these higher NTMP concentrations is due to a decrease in the number of net ionized groups as the solution pH drops. The structural changes of NTMP caused by its deprotonation (dissociation) reactions have been determined <sup>(31-33)</sup> and are shown in Figure 14.

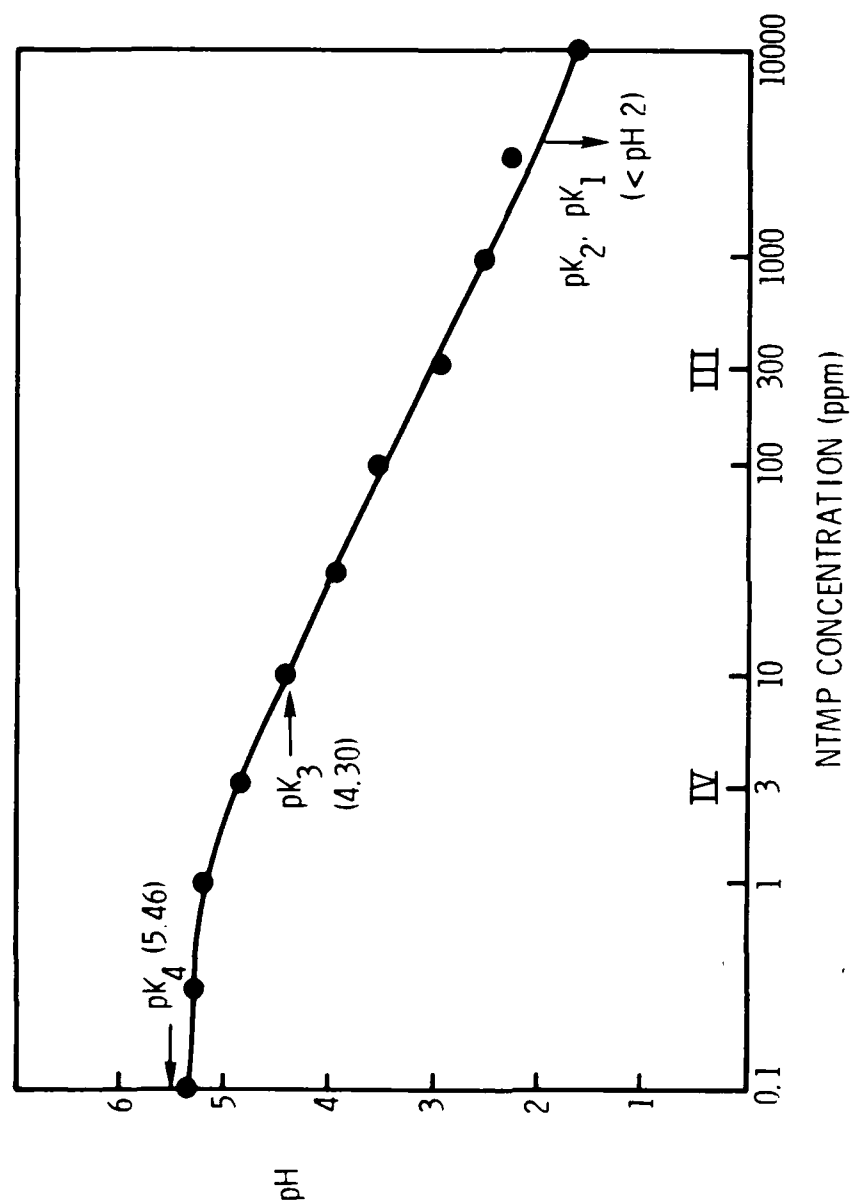


Figure 12. The relationship of pH vs NTMP concentration over a  $pH$  to 10,000-ppm range, including acidity constant values.

Table V

Reported Acidity Constants for Nitrilotris  
Methylene Phosphonic Acid (NTMP)

Acidity Constant	Reported Values		
	Ref. 31	Ref. 32	Ref. 33
pK <sub>1</sub>	<2	0.3 $\pm$ 0.2	1.9
pK <sub>2</sub>	<2	1.5 $\pm$ 0.2	2.0
pK <sub>3</sub>	4.30 $\pm$ 0.05	4.64 $\pm$ 0.05	4.60
pK <sub>4</sub>	5.46 $\pm$ 0.05	5.86 $\pm$ 0.05	5.92
pK <sub>5</sub>	6.66 $\pm$ 0.05	7.3 $\pm$ 0.05	7.35
pK <sub>6</sub>	12.34 $\pm$ 0.14	12.1 $\pm$ 0.15	10.9



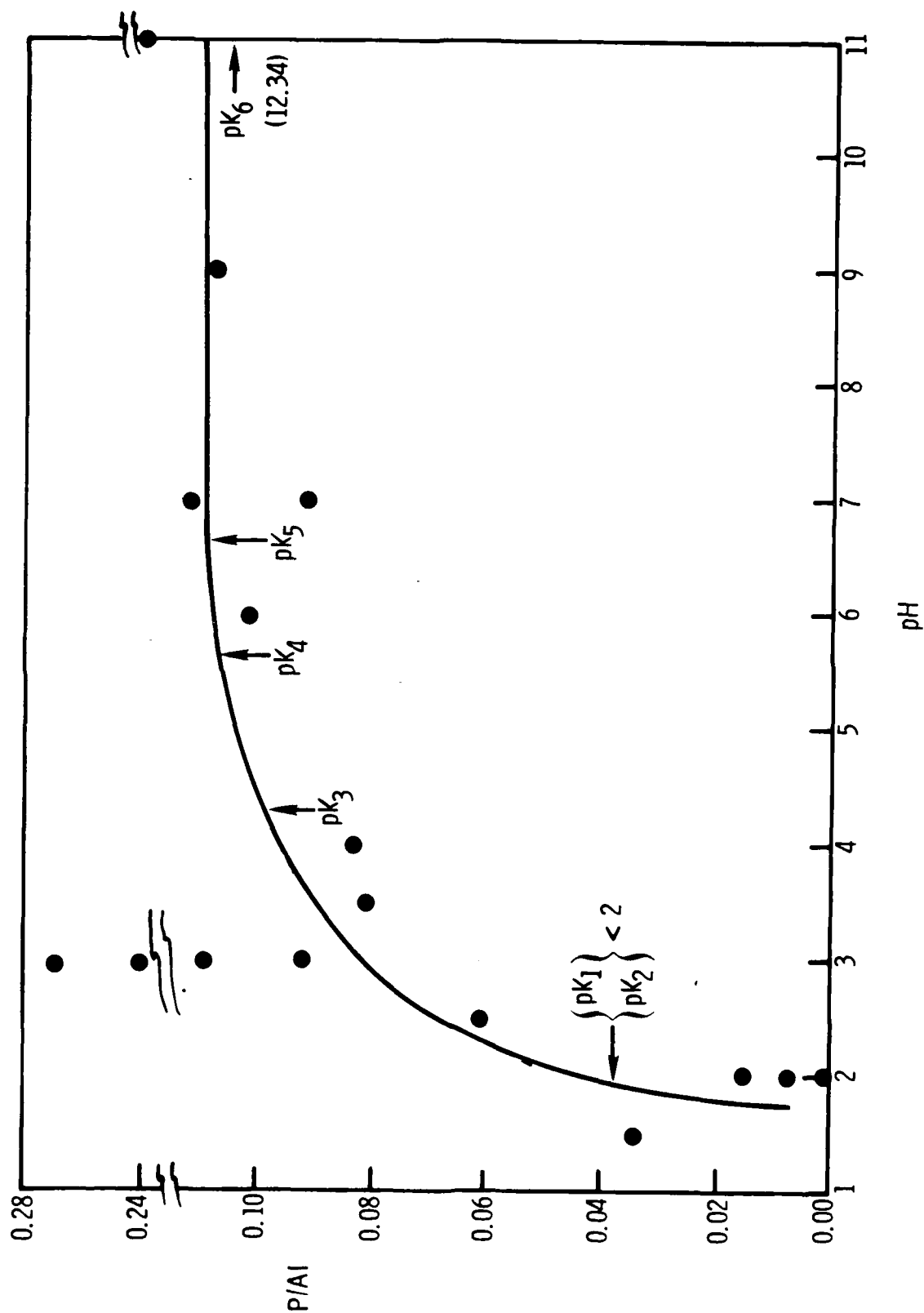


Figure 13. The relationship of the P/Al atomic ratio vs pH for a 100 ppm  $N_3MP$  solution over a pH range of 1.5 to 11. Acidity constant values are also shown.

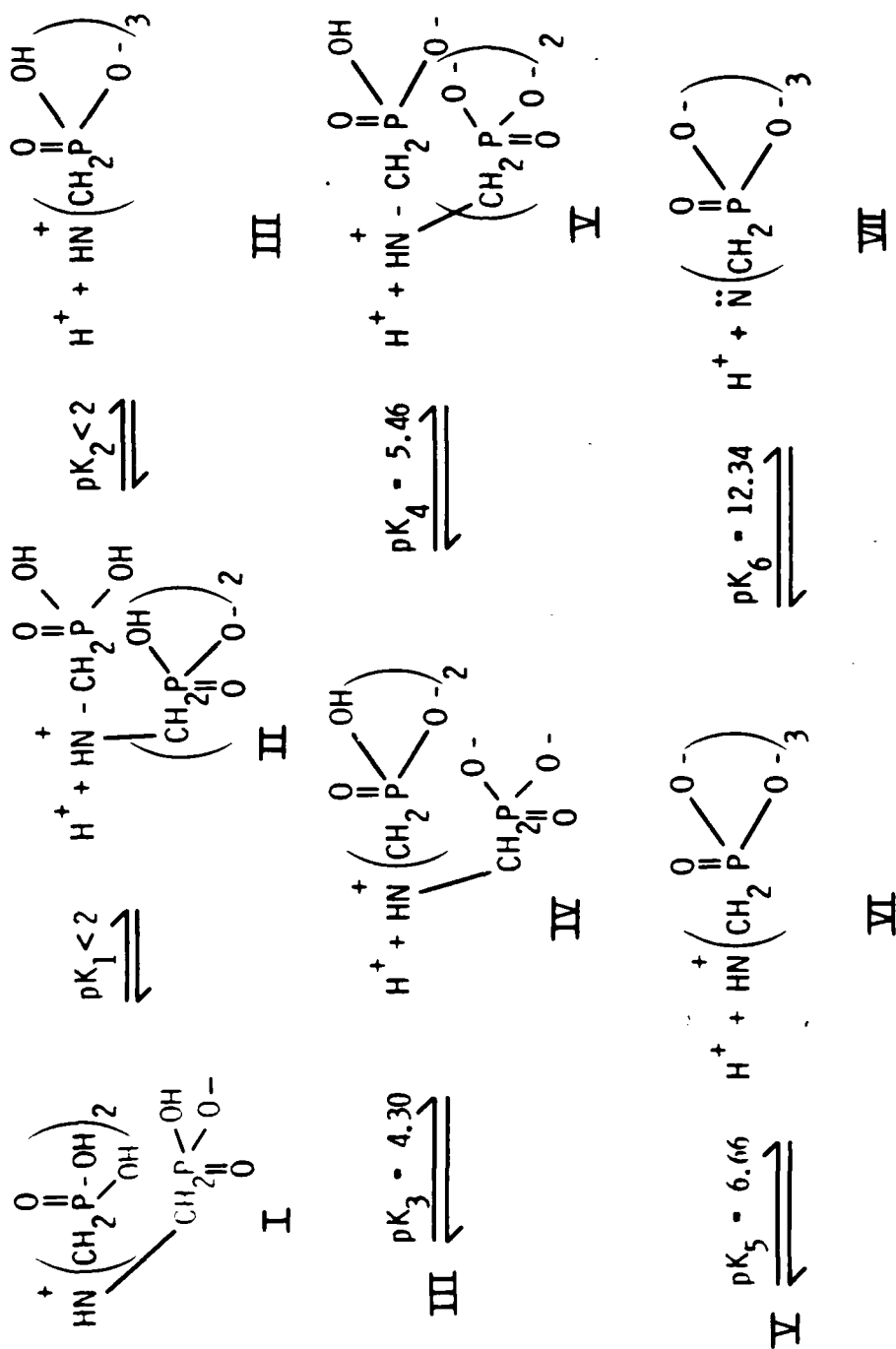


Figure 14. Deprotonation (dissociation) reactions for nitrilotris methylene phosphonic acid (NTMP). (31)

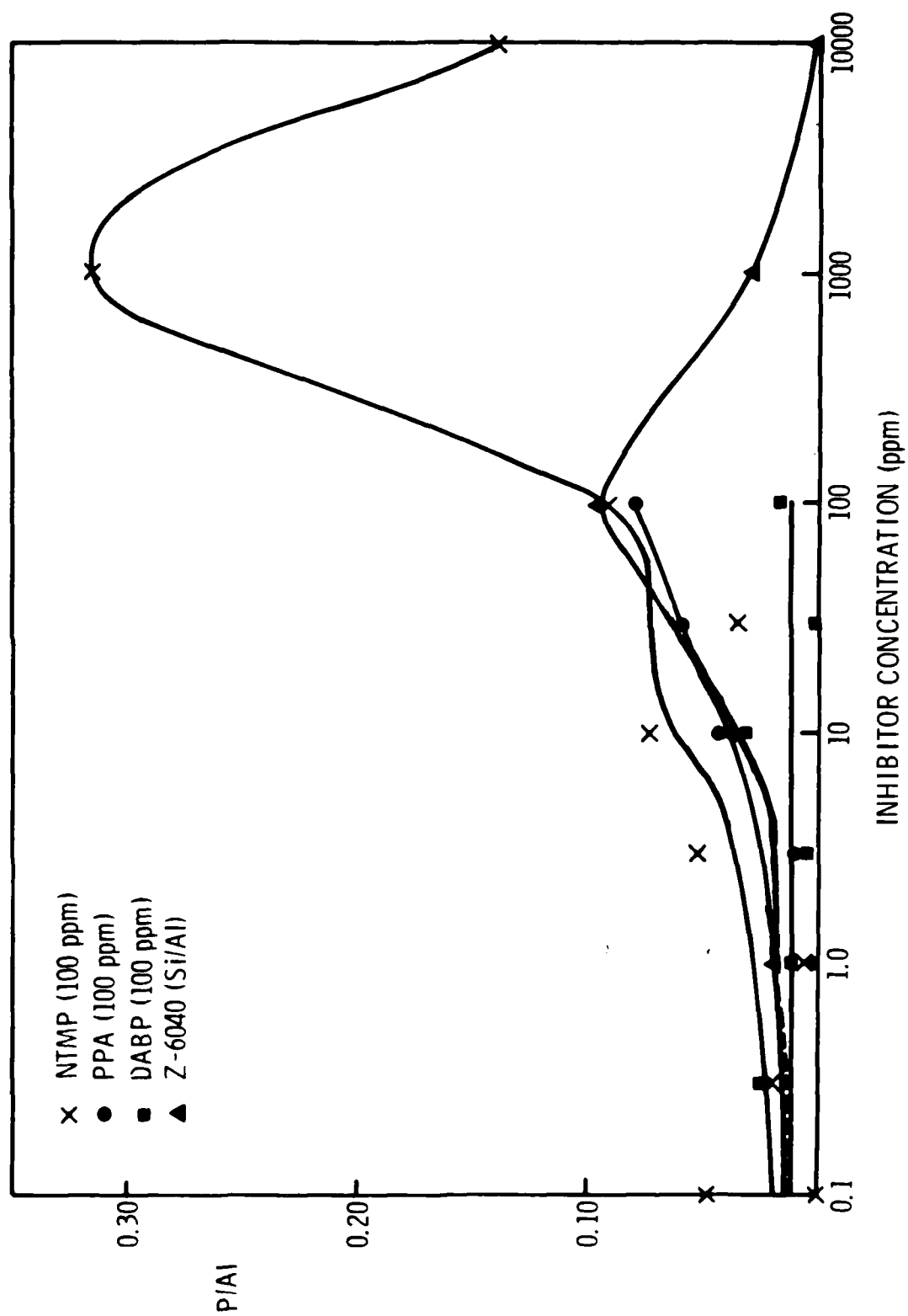


Figure 15. Adsorption of phosphonate and silane inhibitors onto SAA oxide surface.

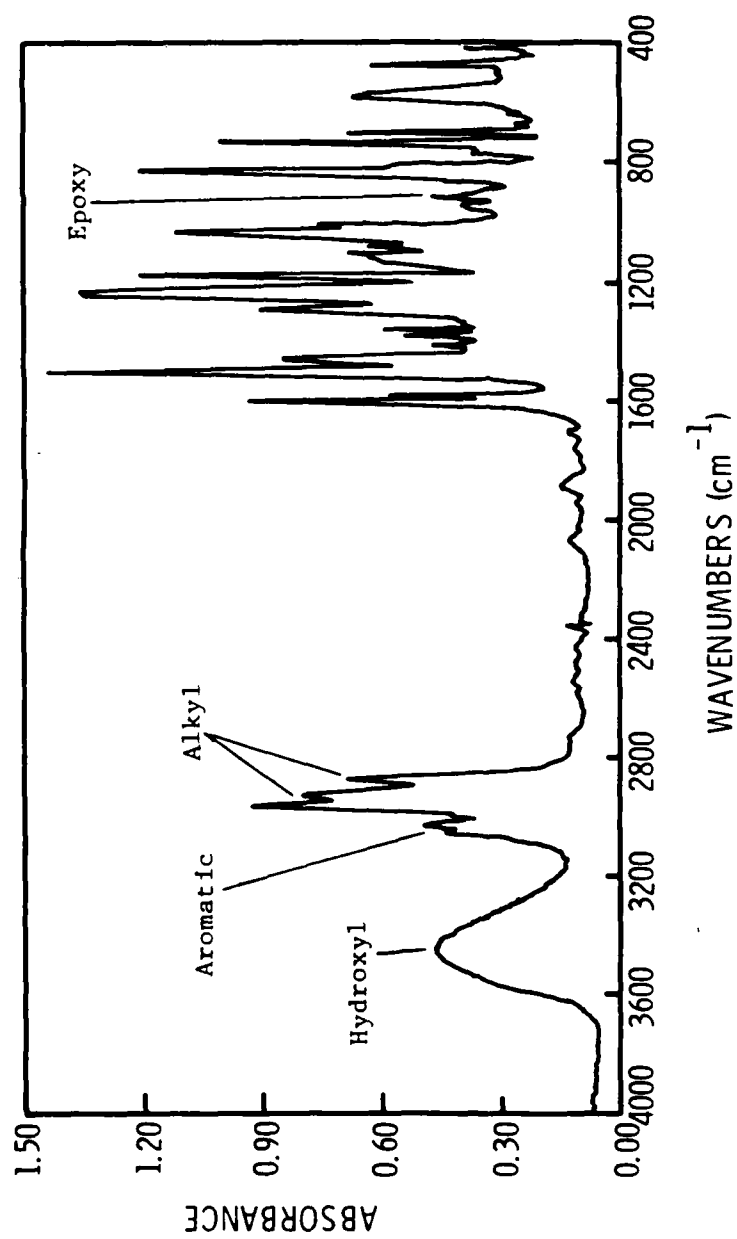


Figure 16. FT-IR spectrum of EPON 1001-T75 epoxide resin.

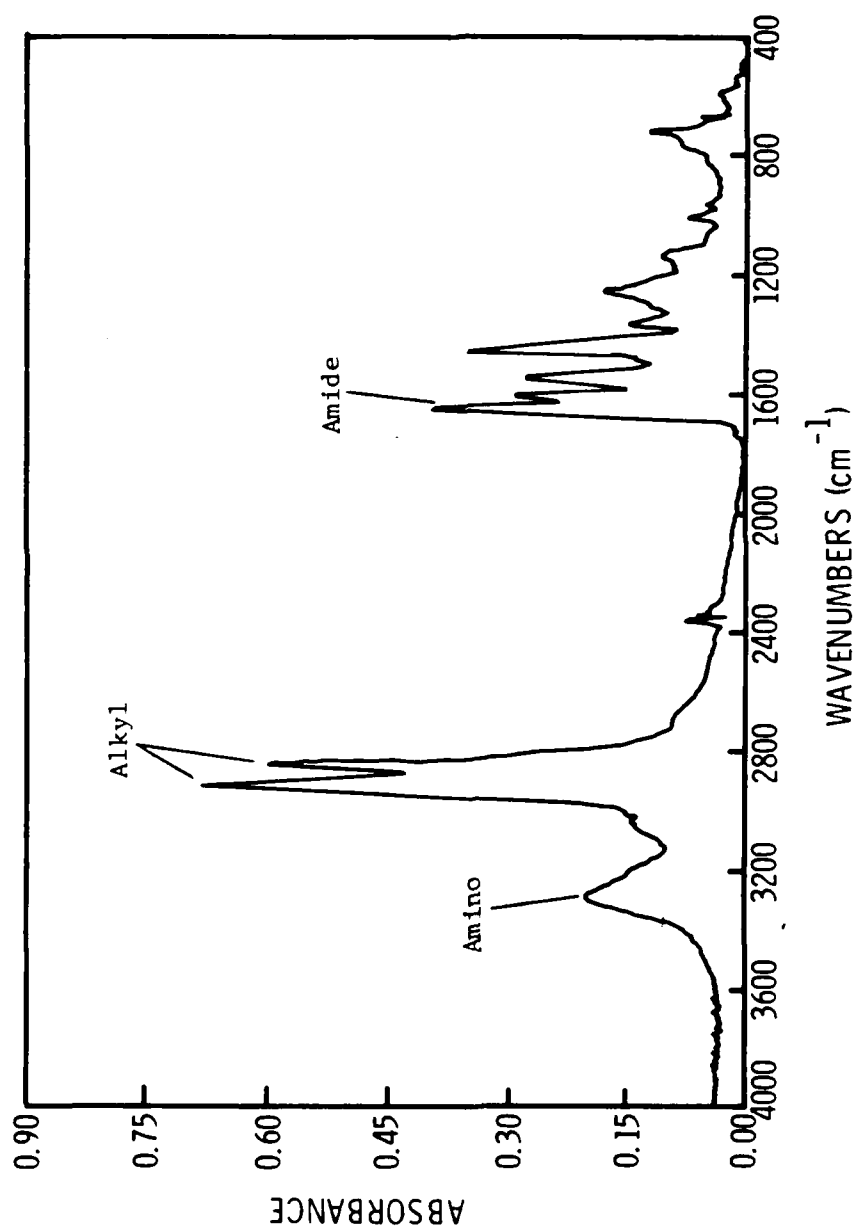


Figure 17. FT-IR spectrum of Versamid 115 polyamide resin.

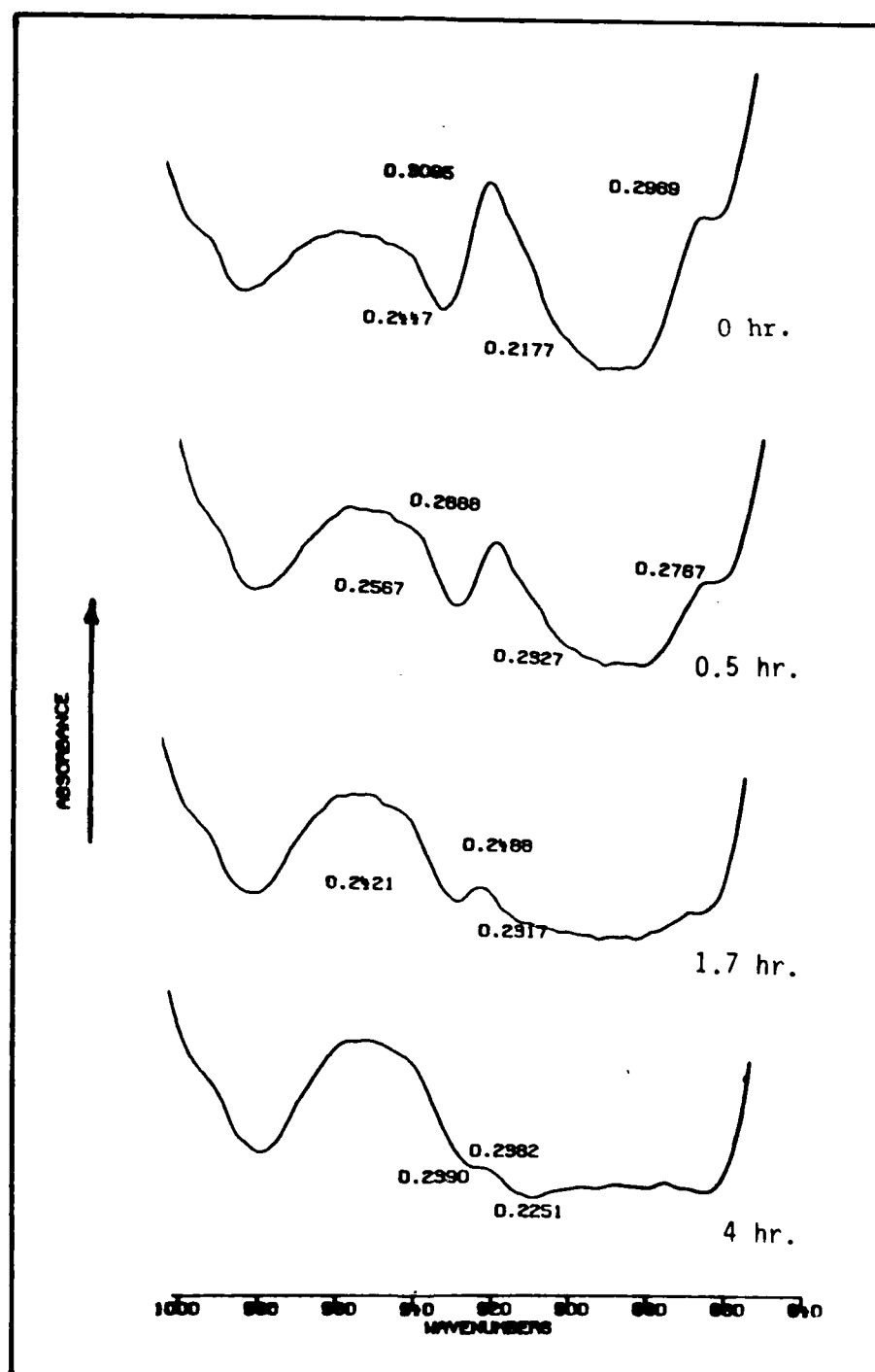


Figure 18. FT-IR kinetics plot of epoxide band ( $917\text{ cm}^{-1}$ ) during epoxy-polyamide curing reaction at  $50^{\circ}\text{C}$ .

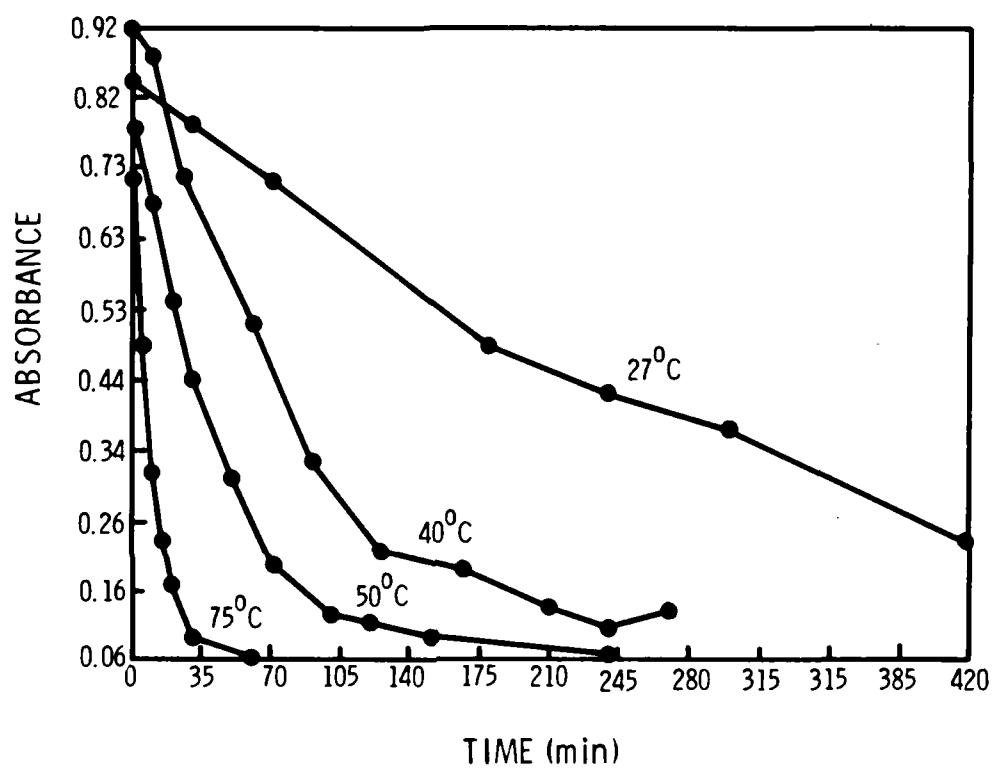


Figure 19. Kinetics plot of FT-IR analysis of epoxy-polyamide curing reaction.

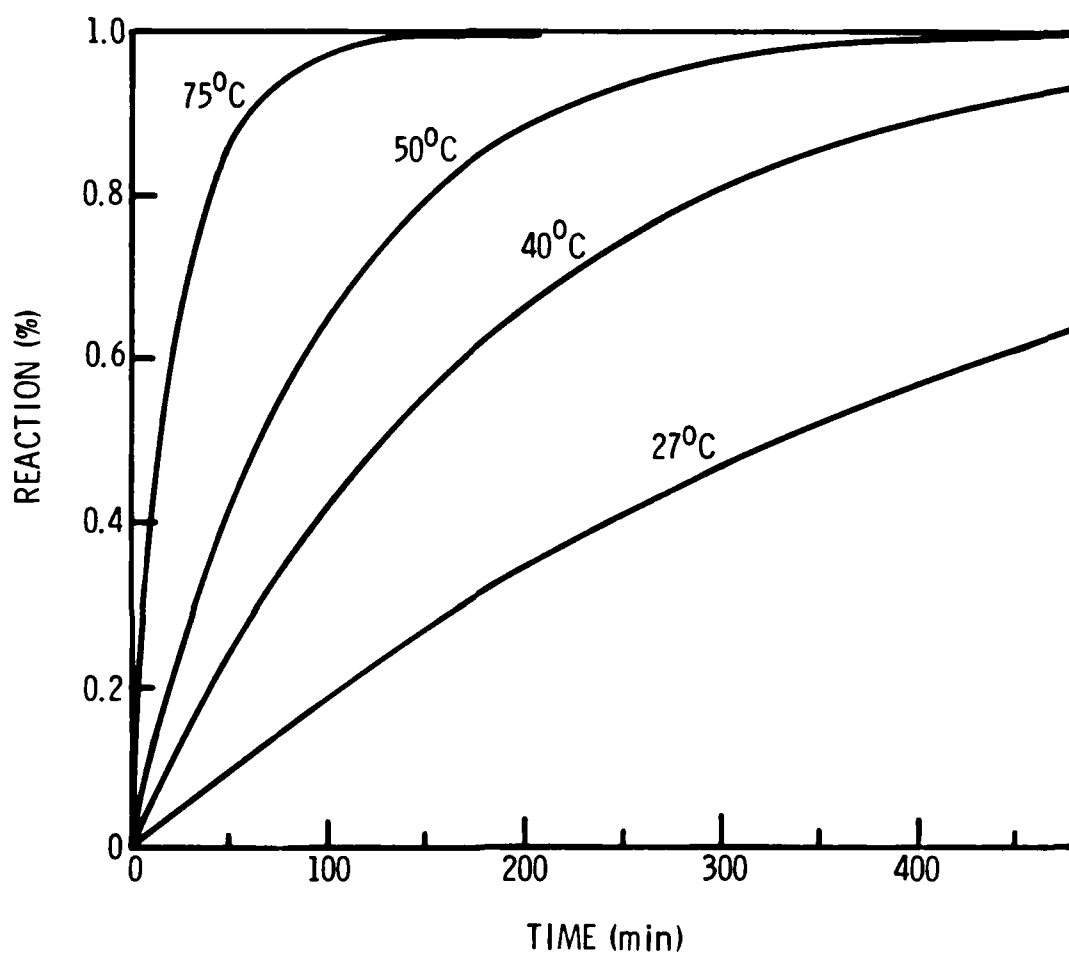


Figure 20. DSC kinetics plot of epoxy-polyamide curing reaction.



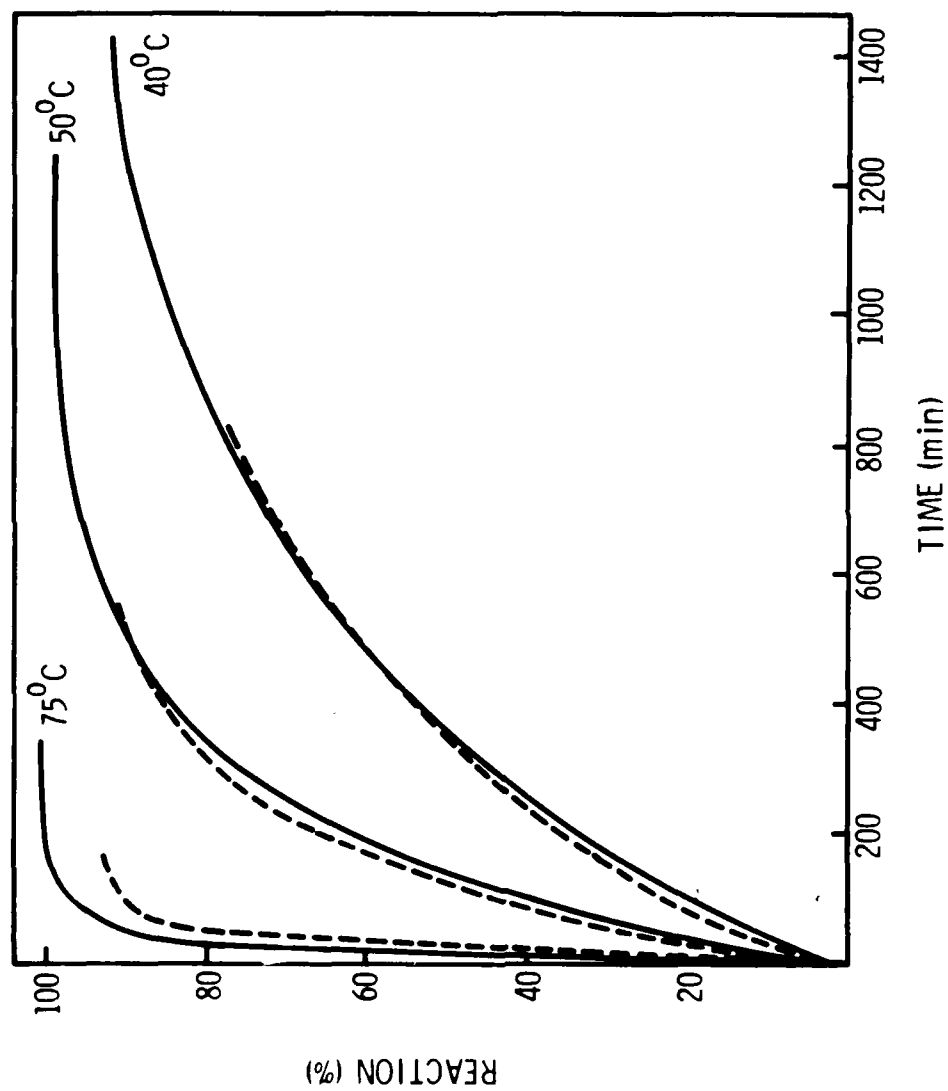


Figure 21. Correlation of FT-IR (---) and DSC (—) kinetics data for epoxy curing reaction.

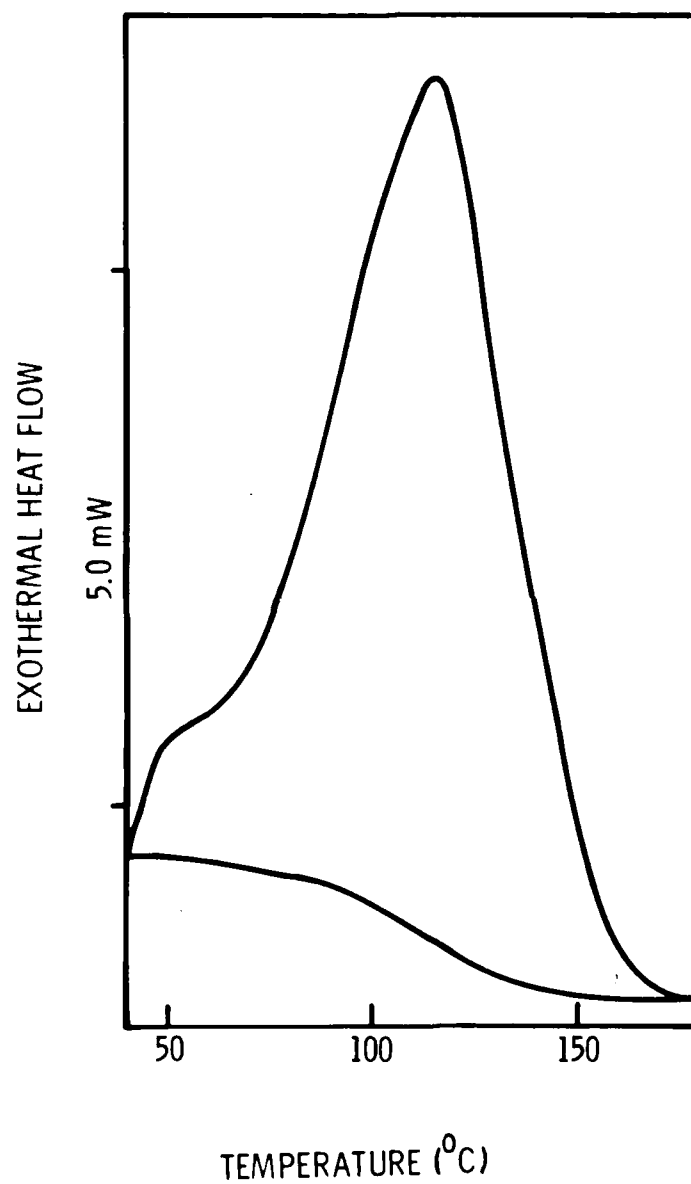


Figure 22. DSC thermal transition curve for epoxy curing-reaction.

(extrapolated from non-isothermal DSC analyses) is illustrated in Figure 20. When normalized to correct for thermal lag effects, the FT-IR curves closely resemble those calculated by the linear DSC process, as shown in Figure 21. The average peak temperature and reaction order were determined to be 118.4°C and 1.08, respectively, by DSC. A typical thermal curve for the curing process is shown in Figure 22.

### 3. Inhibitor Addition to Primer.

Three of five phosphonate inhibitors tested for compatibility with the resin system (PPA, DABP, and DPAP) were readily soluble in the B (isopropanol-containing) component to high concentration levels (above 1000 ppm). Isopropanol formulations of DABP and PPA were subsequently added to the B component prior to application to panels used for corrosion testing, as described. Phosphocreatine (PCR) was found to be only partially soluble and NTMP virtually insoluble in both isopropanol and the B component.

Consequently, NTMP was added to the A-B epoxy system in various suspension forms. Although the kinetics of the normal A + B epoxy-curing reaction were affected by the solvent and solvent-NTMP systems, a "mull" suspension (5 wt%) of solid NTMP in the undiluted A + B mixture did not affect the normal curing process, as shown by the thermal transition curves are illustrated in Figure 23. This finding has significant implications for the phase of this work concerned with incorporation of the inhibitor(s) into the primer system.

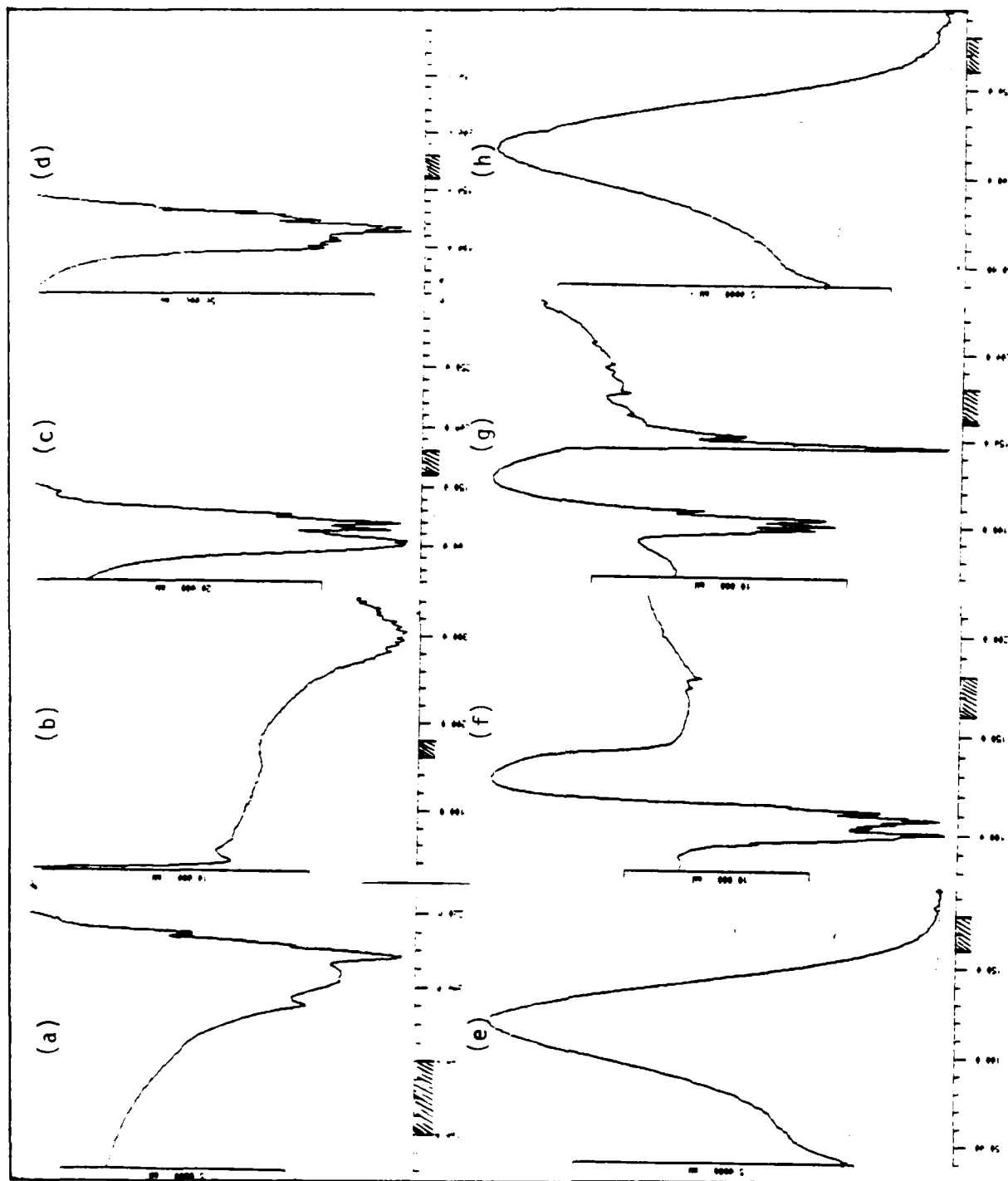


Figure 23. DSC thermal transition curves for inhibitor, solvent and epoxy system: (a) NTMP, (b) B component only, (c) B + iPrOH, (d) B + iPrOH + NTMP, (e) A + B, (f) A + B + iPrOH, (g) A + B + iPrOH + NTMP, and (h) A + B + NTMP null. The 160-180°C range is indicated by cross-hatching on each scale.

Table VI

Corrosion Salt-Fog Results on 7075-T6 Test Panels

Treatment	Facility	Inhibitor Adsorption			Primer	Exposure Time (hr.)	Final Appearance
		Compound	Conc. (%)	Solvent			
SAA	Lab	Control (none)	-	-	Fig.	1250	No blisters
SAA	Lab	Control	-	-	Unpig.	1250	No blisters
SAA	Lab	NTMP <sup>a</sup>	0.5	M:W <sup>b</sup>	Unpig.	1250	No blisters
SAA	Lab	A-0800 <sup>c</sup>	0.5	M:W	Unpig.	1250	No blisters
SAA	Lab	DABP <sup>d</sup>	0.5	iPrOH <sup>e</sup>	Unpig.	1250	No blisters
SAA	Lab	PPA <sup>f</sup>	0.5	iPrOH	Unpig.	1250	No blisters
CCC	Lab	Control	-	-	Fig.	1250	Mod. blistering
CCC	NADC	Control	-	-	Fig.	1000	Little blistering
CCC	Lab	Control	-	-	Unpig.	1250	Mod. blistering
CCC	NADC	Control	-	-	Unpig.	1000	Little blistering
CCC	Lab	NTMP	0.5	M:W	Unpig.	1250	Mod. blistering
CCC	NADC	NTMP	0.5	M:W	Unpig.	1000	Severe blistering
CCC	Lab	A-0800	0.5	M:W	Unpig.	1250	Mod. blistering
CCC	NADC	A-0800	0.5	M:W	Unpig.	1000	Little blistering
CCC	Lab	DABP	0.5	iPrOH	Unpig.	1250	Mod. blistering
CCC	NADC	DABP	0.5	iPrOH	Unpig.	1000	Little blistering
CCC	Lab	PPA	0.5	iPrOH	Unpig.	1250	Mod. blistering
CCC	NADC	PPA	0.5	iPrOH	Unpig.	1000	Little blistering

<sup>a</sup> NTMP = Nitrilotris methylene phosphonic acid<sup>b</sup> 50 parts MeOH: 50 parts H<sub>2</sub>O (vol:vol)<sup>c</sup> A-0800 =  $\gamma$ -aminopropyltrimethoxysilane<sup>d</sup> DABP = diethyl p-aminobenzylphosphonate<sup>e</sup> Inhibitor was added to epoxy B component as iPrOH solution prior to mixing of primer components for spraying.<sup>f</sup> PPA = Phenylphosphonic acid

## D. CORROSION TESTING

### 1. Salt-Fog Test.

Bare 7075-T6 panels, prepared by SAA and chromate conversion coating (CCC) methods, were treated with inhibitor solutions and subjected to salt spray (fog) testing (ASTM B-117). According to the results summarized in Table VI, anodized (SAA) 7075-T6 Al is extremely resistant to salt-initiated (5% NaCl) corrosion for at least 1200 hours. Only residual salt remained along the scribe marks following the exposure period. The oxide produced by the SAA process demonstrates such superior anticorrosive properties that a rapid, practical evaluation of inhibitor compounds by the standard salt-fog method is not possible.

The non-anodized CCC panels (See Section II A) generally displayed a poorer resistance to salt-initiated corrosion than the comparable SAA-prepared specimens. Corrosion bubbles appeared consistently on all CCC panels tested at the Labs (1250 hr). Although the CCC panels tested at NADC (1000 hr) generally indicated a lesser degree of blistering than the corresponding Labs specimens, the exposed NTMP-treated panels had a high density of corrosion bubbles. Representative photographs of the NTMP-adsorbed test panels, before and after their salt-fog chamber exposure period, are shown for SAA (Labs), CCC (Labs) and CCC (NADC) specimens in Figures 24, 25, and 26, respectively. The quantitative NADC results are reported according to the ASTM 2197-B adhesion rating system in Table VII.

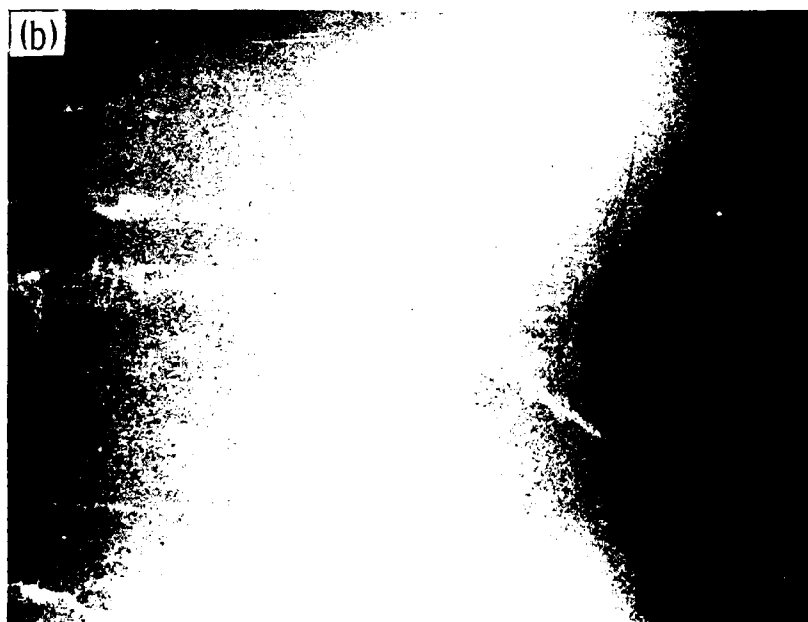
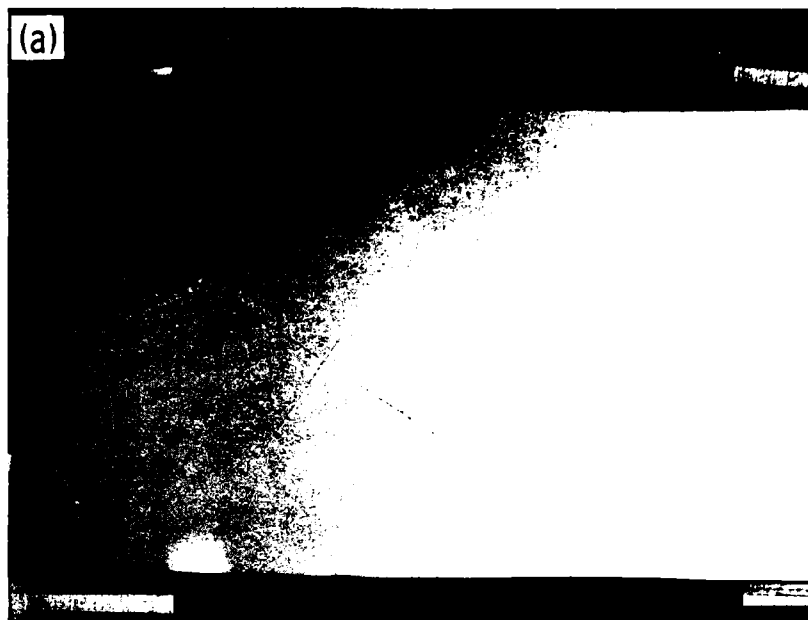


Figure 24. Photographs of Martin Marietta Laboratories test panel: SAA treated with NTMP (5000 ppm) (a) before and (b) after exposure in salt-fog chamber (1250 hr).

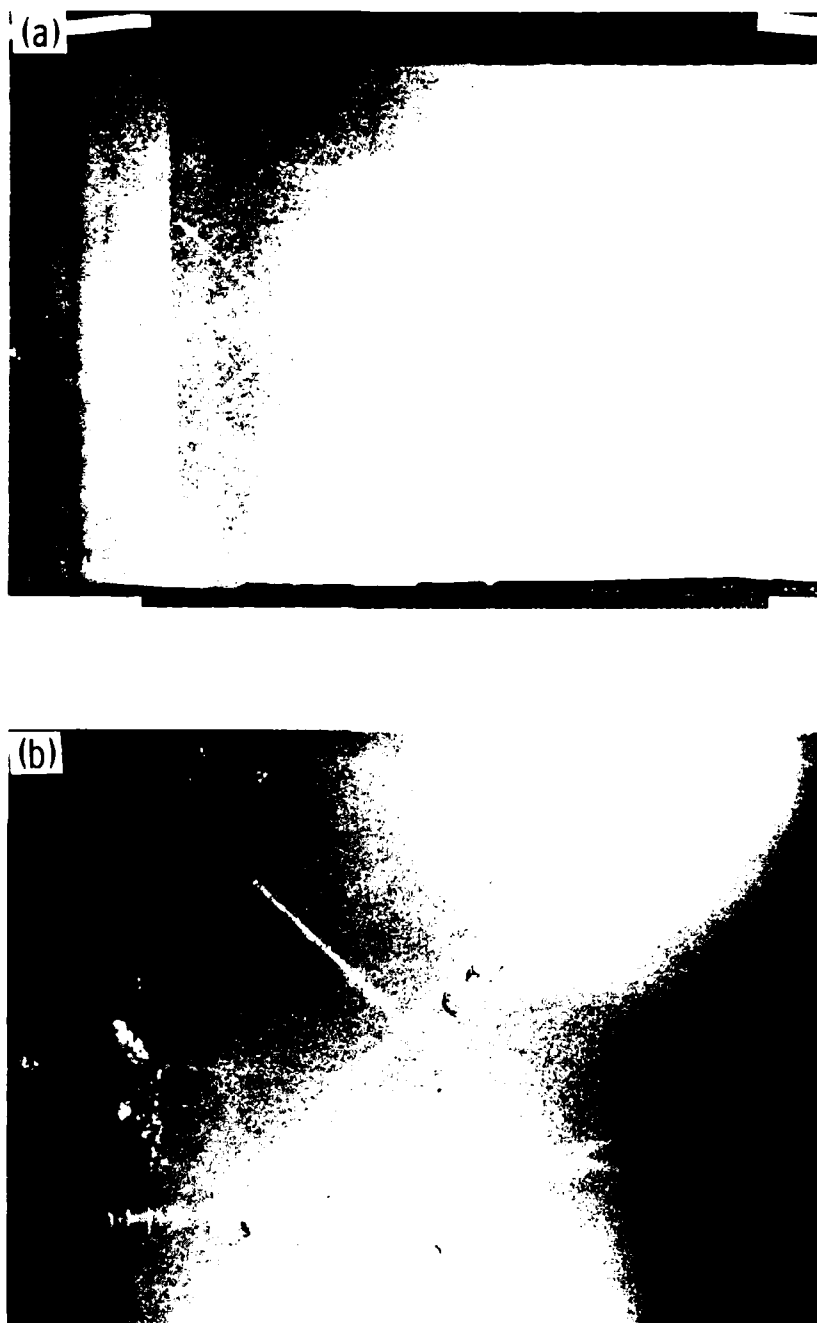


Figure 25. Photographs of Martin Marietta Laboratories test panel: CCC treated with NTMP (5000 ppm) (a) before and (b) after exposure in salt-fog chamber (1250 hr).





Figure 26. Photographs of duplicate NADC test panels: CCC treated with NTMP (5000 ppm) after exposure in salt-fog chamber (1000 hr).

Table VII

Corrosion Salt-Fog Results for NADC Chromate Conversion  
Coated (CCC) Specimens by ASTM 2197-B Rating System

<u>Specimen-Inhibitor</u>	<u>500 hr</u>	<u>Appearance 1000 hr</u>	<u>Adhesion* (mils)</u>
Control-pigment	OK	OK	5
Control-pigment	OK	OK	3
Control-unpigmented	OK	{ Slight blistering above scribe Corrosion in scribe }	6
Control-unpigmented	OK		6
NTMP 50/50	Corrosion initiation Corrosion initiation Corrosion initiation	{ Many corrosion areas in and away from scribe }	9
NTMP 50/50			9
NTMP 50/50			19
PAA Bare	OK	Slight corrosion in scribe Slight corrosion in scribe	8
PAA Bare	OK		8
DABP	OK	Slight corrosion in scribe Slight corrosion in scribe	8
DABP	OK		8

\*Lowest number indicates least corrosion

## 2. Wedge Test.

Corrosion inhibitor compounds were also evaluated by the wedge-test procedure, which accelerates the metal-adhesive debonding process by the application of a stress normal to the primer-oxide interface. The final crack length extensions are a measure of the ability of the compounds to inhibit hydration of the oxide. Subsequent examination of the debonded surfaces with XPS and XSEM indicates the type of bond failure, i.e., adhesive (between the adhesive and oxide surfaces) or cohesive (within the adhesive or oxide).

Initial attempts to use the epoxy primer as the adhesive for these tests were unsuccessful because the primer would not cure completely. Consequently, a chemically similar epoxy-based structural adhesive, FM-123-2, was substituted. Earlier investigations using NTMP showed that this inhibitor provides equivalent bond performance with several epoxy-based adhesives.<sup>(34,35)</sup>

The initial wedge-test results demonstrated good performance by the SAA control and equivalent performance by SAA panels treated with Z-6040 (5000 ppm) and a 100-ppm solution of NTMP, as shown by the crack extension vs time relationship in Figure 27. Higher solution concentrations of NTMP, on the other hand, degraded bond durability.

A second wedge test, in which lower NTMP and Z-6040 solution concentrations (2-200 ppm) were evaluated as well as two new inhibitors (PPA and A-0800), was then performed. The results, presented in Figure 28, indicate that each inhibitor system demonstrated adhesion durability properties equivalent to those of the SAA control.

The failure analysis of the wedge-test specimens is still in progress and the results will be reported in detail in future reports. Initial results, such as the XPS analysis of Table VIII, indicate that the locus of failure of these

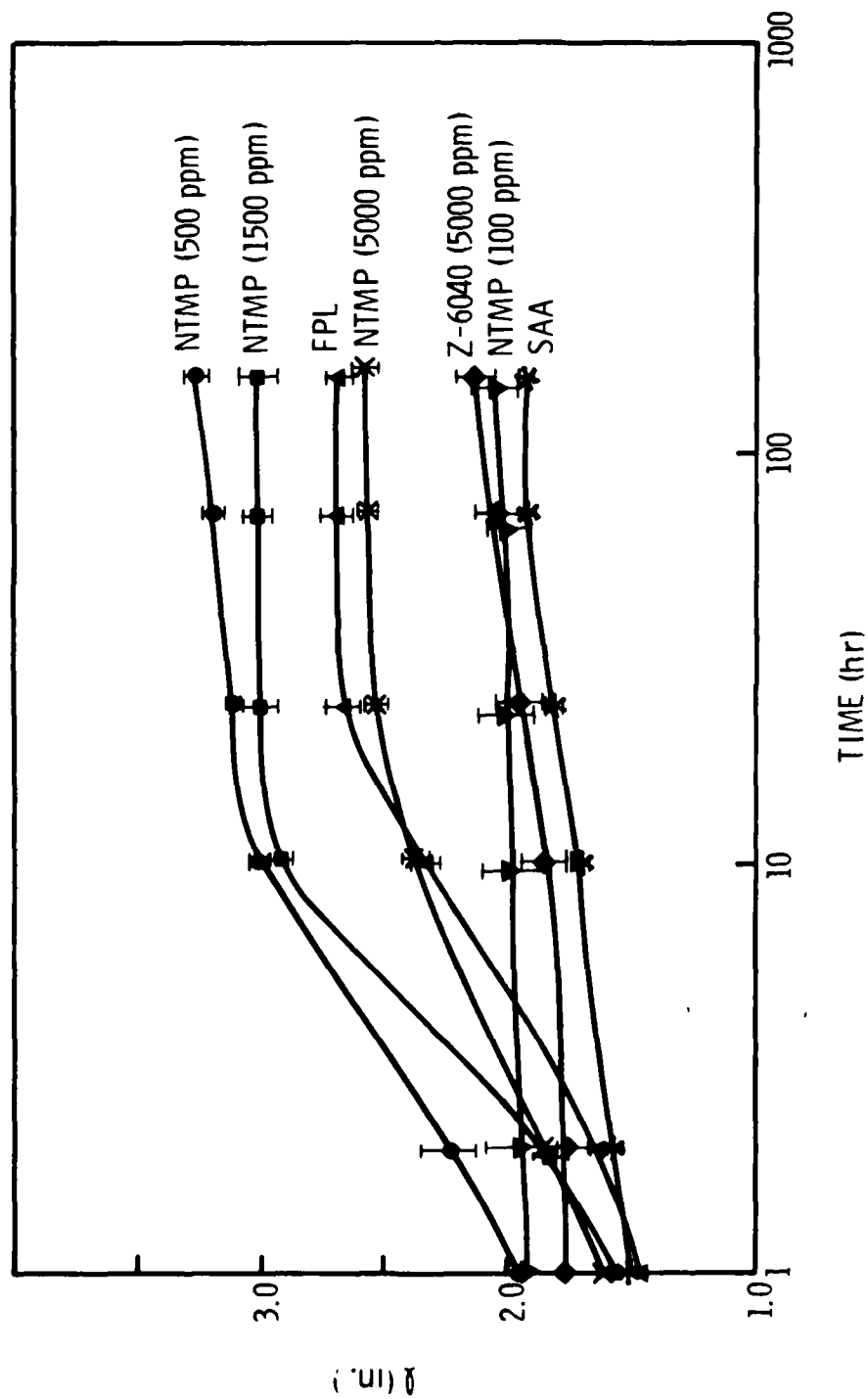


Figure 27. Crack length vs time curve for wedge test using various specimen treatments.

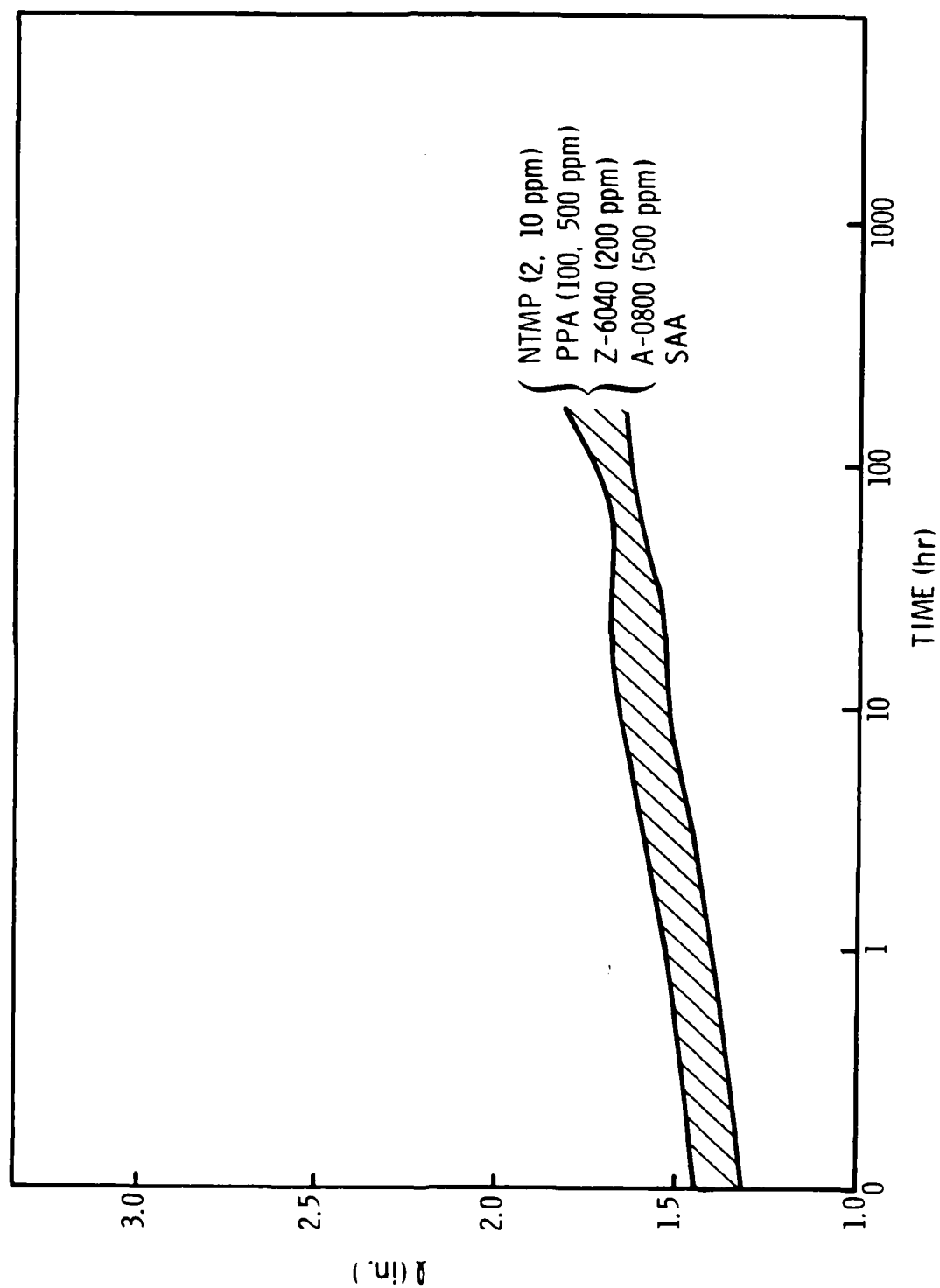


Figure 28. Crack length vs time curve for wedge test using various specimen treatments.

Table VIII

## XPS Analysis of Adjoining Side of Wedge Test Panels

Treatment	Atomic %							
	<u>Al</u>		<u>O</u>		<u>C</u>		<u>Other</u>	
	<u>M*</u>	<u>A*</u>	<u>M</u>	<u>A</u>	<u>M</u>	<u>A</u>	<u>M</u>	<u>A</u>
FPL	30	29	56	58	14	13	-	-
SAA + NTMP (5000ppm)	20	4	42	22	31	70	P 1.0 S 0.5	N 3 Si 1 P 0.3 S 0.4
SAA	25	28	56	56	19	16	-	-
SAA + NTMP (100ppm)	0.5	1	19	18	76	76	N 3 Si 1 S 0.4	Si 1 S 0.3
SAA + Z-6040 (5000ppm)	18	14	44	37	37	47	Si 1	N 2

\*M = metal side, A = adhesive side

bonds differs even between samples exhibiting similar wedge-test performance. The FPL-treated samples fail as the oxide hydrates, leading to failure at the hydroxide-metal interface and subsequent hydration of the metal surface.<sup>(3)</sup> (The 14% C on each of these surfaces results from adventitious hydrocarbons and represents a baseline for C concentration.) Similar results are also seen for the SAA control. In this case, because of the increased thickness of the oxide and the tendency for only the surface regions of the SAA oxide to hydrate, crack propagation is likely to occur within the oxide and not at the oxide-metal interface.

The remaining samples analyzed exhibit still other modes of failure. Bondments treated with solutions of high concentrations of NTMP (5000, 1500, and 500 ppm) apparently failed adhesively between the oxide and the adhesive, as indicated by the high concentrations of Al and O (C) on the metal (adhesive) sides of the failure. The detection of P suggests that crack propagation occurs primarily along the inhibitor-adhesive interface or through the inhibitor multiple layer. In contrast, the samples treated with the 100-ppm NTMP solutions exhibit high (low) concentrations of C (Al) on both sides, indicating crack propagation cohesively within the adhesive. Nonetheless, the locus of failure must be near the interface since the "metal" surface looks metallic and not purple like the adhesive. Finally, the Z-6040-treated panels have moderate levels of both Al and C. Bond failure here appears to be mixed-mode, possibly within the oxide region, where the adhesive penetrates down into the pores. Alternatively, the crack may have propagated adhesively and cohesively at different points within our analysis region

(1- to 3-mm in diameter) or the inhibitor coverage may have been incomplete due to less than optimal solution conditions employed (See Figure 15).

Initial analysis using XSEM supports the XPS findings. However, further work is needed (and is continuing) to choose between the two possible failure mechanisms for the Z-6040 bondments and to develop a fuller understanding of crack propagation for the complete set of inhibitors tested.



#### IV. DISCUSSION

##### A. FRESH SAA OXIDE

The morphology of our SAA oxides, which was illustrated in Figure 5, is very similar to that reported by others using somewhat different anodization conditions.<sup>(12,21-23)</sup> The results serve as a baseline for subsequent hydration, adsorption, and bonding experiments.

The greater thickness of the SAA oxide, compared to most other oxides on aluminum, affords the substrate greater protection from the environment (hydration or sealing can provide even greater protection, as discussed below). The porous nature of the oxide, though less open than the oxide produced by the two surface preparations conventionally used for structural adhesive bonding -- phosphoric acid anodization (PAA) or dichromate-sulfuric acid (FPL) etching -- allows micromechanical interlocking between the oxide and an applied polymer, provided that the polymer penetrates into the oxide.<sup>(12)</sup> As we will see, the oxide thickness and microroughness combine to make painted SAA surfaces very resistant to environmental degradation.

Chemically, the SAA surface was found to be  $\text{Al}_2\text{O}_3$  with the equivalent of approximately one monolayer of  $\text{Al}_2(\text{SO}_4)_3$ . The measured S/Al ratio of  $\sim 0.08 - 0.1$  corresponds to the 11 - 14 wt.% value reported for sulfate ( $\text{SO}_4$ ), obtained by analytical chemistry techniques,<sup>(21,22,36)</sup> if the sulfate is incorporated more or less uniformly throughout the oxide.<sup>(22)</sup> In many cases, varying quantities of adsorbed water can also be detected on the surface. From our previous work,<sup>(19,26,27)</sup> this water is physisorbed in a quantity dependent on the storage conditions and can be easily removed by placing the sample in a dehydrating environment such as a dessicator or a vacuum.

## B. HYDRATION

After our samples are immersed in 80°C water for several minutes, a hydration product grows on the surface to fill the pores and "mud cracks" of the original oxide. This is one variation of the "sealing" operation frequently used to improve corrosion resistance by producing a dense, thick oxide/hydroxide layer to physically separate the metal from its environment.<sup>(21,36-38)</sup> Hydration of SAA oxides may be beneficial from a corrosion point of view, but the process can be very detrimental with regard to adhesion.<sup>(6,12,13)</sup> For example, hydration after bonding induces stresses at the oxide (hydroxide) polymer interface due to dramatic morphological and volume changes of the oxide. Additionally, at least for thin oxides where the entire oxide hydrates, poor adherence of the hydroxide to the metal allows bond failure at this interface. Bonding after cessation of the hydration eliminates the stresses due to morphological and volume changes. However, because the microroughness of the surface is greatly reduced (the surface area decreases to 1% of its initial value<sup>(36)</sup>), the micromechanical interlocking required for good adhesion properties is diminished.\* Our wedge-test results (to be discussed below) support this contention by demonstrating that crack propagation occurs with untreated SAA adherends which the oxide hydrates.

According to the results of surface analysis, the behavior of hydrated SAA surfaces is similar to that of PAA surfaces:<sup>(26)</sup> physisorption of water (discussed above) and growth of boehmite ( $\text{AlOOH}$ ) on the surface. No subsequent

---

\*In certain cases a controlled "sealing" of SAA surfaces in chromic acid will enlarge thin pores to allow more polymer to penetrate. This increased interlocking effectively improves the adhesion of paints.<sup>(39)</sup>

hydration to bayerite  $\text{Al}(\text{OH})_3$  was observed on the SAA surfaces; however, it is possible that the longest hydration time was too short for this step to occur. The evolution of the surface composition directly to boehmite could be caused by (1) a slow dissolution of the sulfate followed by a rapid hydration of  $\text{Al}_2\text{O}_3$  to  $\text{Al}(\text{OH})_3$ , or (2) the growth of  $\text{Al}(\text{OH})_3$  on top of the sulfate. In our study of PAA oxide, it was determined that phosphate dissolution is the limiting step in the hydration process. However, we cannot distinguish between these two possibilities for the SAA oxide, because such a detailed study of the SAA hydration is beyond the scope of this program.

### C. ADSORPTION

Previous investigations of inhibited FPL and PAA surfaces have demonstrated that a monolayer of NTMP, the optimal coverage for bond durability, is readily achieved with immersion in solutions of  $\geq 10$ -ppm concentration.<sup>(16,18)</sup> Corresponding measurements on treated SAA samples demonstrate similar behavior following their immersion in solutions of  $\leq 100$ -ppm NTMP. (The somewhat lower P/Al value for treated SAA surfaces compared to treated PAA and FPL surfaces probably reflects a difference in the density of active adsorption sites.) At higher NTMP concentrations ( $\sim 1000$  ppm), however, multiple layer coverage is achieved -- a phenomenon not observed with other aluminum surfaces treated in NTMP solutions up to 500 ppm. Such behavior may be due to the changes in the NTMP structure as the pH of the solution drops (Figures 12 and 13). At extremely low pH, there is very little adsorption from solution. However, by  $\sim \text{pH } 3.5$ , NTMP coverage has risen to a P/Al of  $\sim 0.10$ , where it remains constant as the pH is increased. Such results suggest that the

adsorption behavior observed as the concentration of NTMP (a multiprotic acid) increases is correlated with to a net decrease in the number of ionized functional groups as the concomitant solution pH drops. In two cases, coverage levels obtained at pH 3 from subsequent experimental runs were found to be higher (~twofold) than the initial coverage values suggesting a possible multilayer inhibitor coverage at this pH.

While additional measurements are scheduled to confirm these findings, and empirical correlation between the NTMP structure and adsorption phenomena can be noted. A comparison of Figures 13 and 14 shows that monolayer coverage is obtained in the presence of structure IV and more deprotonated forms (assuming a sufficient population to successfully compete with water for adsorption sites). As the concentration of structure III becomes significant,<sup>(32)</sup> however, a multiple layer of NTMP molecules or Al-NTMP complex(es) begins to form, possibly due to enhanced intermolecular H-bonding which is a result of the stable conformation (symmetry) of the molecules. Finally, adsorption decreases as structure II begins to dominate. Evidently, the increased intramolecular H-bonding and reduced symmetry allow less bonding between the NTMP molecules and, apparently, less bonding to the aluminum oxide substrate.

This correlation between NTMP structure and its adsorption onto SAA surfaces, while very plausible, cannot yet be considered established. However, the results do indicate the importance of pH to the adsorption process and the need to maintain proper control over solution parameters.

#### D. INHIBITOR INCORPORATION INTO PRIMER

The incorporation of inhibitors into the two-component epoxy resin system depends on the solubility properties of the compound in the final solvent system. Of the four primary solvents in the resin system, isopropanol (24.5 final wt.% and 63% of component B) was chosen as the initial solvent vehicle for solubilization of the phosphonate compounds. This process has been successfully used to apply the primer coating to 7075-T6 panels for corrosion testing.

The fact that the three readily soluble phosphonates (PPA, DABP, and diethyl phenethyl-amido-phosphonate, DPAP) all possess a significant organic (nonpolar) character is a direct result of their structural correlation with the relatively nonpolar isopropanol. On the other hand, the more polar (less organic content) NTMP and phosphocreatine (PCR) were rendered less soluble in the isopropanol.

As the range of candidate phosphonate, sulfonate, and silane inhibitors is expanded, it is apparent that additional solubilizing vehicles will be required, particularly for the more polar compounds. The likely solvent is ethylene glycol monoethyl ether (EGMEE), the A component constituent, which comprises 16.4 wt.% of the final mixed resin system. Inhibitor solubility tests in this solvent will commence during the next quarter.

## E. CORROSION TESTING

### 1. Salt-Fog Tests

The results demonstrate that the protective oxide produced by the SAA process is very resistant to salt-induced corrosion. Consequently, the use of the standard salt-fog test surface does not provide an effective evaluation of inhibitor compounds. The alternatives include changing the surface preparation to a milder, well-characterized process such as FPL and/or increasing the severity of the atmospheric fog conditions. The FPL surface treatment is currently being used for the inhibitor testing experiments.

The results of inhibitor evaluation obtained with the non-anodized conversion-coated (CCC) panels (Table VI) must be interpreted carefully. Although the three phosphonate-treated specimen groups had poorer adhesion ratings than both the pigmented and unpigmented controls, the adsorption conditions might not have been optimal. For example the 0.5% (5000 ppm) NTMP solution, which is a standard concentration used for silane couplers as adhesion promoters, was 50-fold more concentrated than the desirable monolayer-forming level (100 ppm, Figure 11) and well into the poor-adsorption pH range (below pH 3, Figure 13). (The optimal adsorption conditions were determined subsequent to this salt-fog test.) Studies involving the adsorption properties of organic inhibitors onto chromic acid surfaces, which may not be equivalent to those for the SAA oxide, are beyond the scope of this work and have not been observed in the literature.

Thus, although the ASTM B-117 method must be utilized as part of any final evaluation of selected corrosion inhibitors, current inhibitor

effectiveness must be determined by a more rapid and efficient screening system. Such experiments are now in progress, as described in Section V.

## 2. Wedge Tests

Because the salt-fog experiments proved inadequate for testing the effectiveness of the inhibitors in reducing corrosion, wedge tests were also used for evaluation. These tests, which apply a stress to the polymer-oxide interface, would be expected to be a more sensitive measurement of the corrosion protection in the absence of a high concentration of aggressive ions.

The wedge tests clearly show the importance of monolayer coverage of NTMP. Bonds prepared with adherends with the highest NTMP coverages (500- and 1500-ppm concentrations) exhibited the poorest resistance to crack propagation. Conversely, those treated with a monolayer coating of NTMP (100 ppm) exhibited very good bond durability, whereas the intermediate coverage of NTMP (5000 ppm) resulted in poor bond performance. Results of the second wedge test, in which lower inhibitor concentrations were examined, further support this correlation. In both cases, as with the salt-fog experiments, measurement of the final crack length indicates that the performance of the SAA control is too good to allow an adequate test of the relative effectiveness of the best inhibitor treatments (100-ppm NTMP, PPA, Z-6040, and A-0800). On the other hand, improvements due to the 100-ppm NTMP treatment may be indicated by slow propagation of the crack once the samples were placed in the humidity chamber (Figure 27). A fracture energy analysis of these data is needed to verify this preliminary observation and is planned for the first part of the second year.

Despite this insensitivity of the crack-length measurements, determination of the locus of failure does allow some evaluation of the inhibitor treatments. Crack propagation for the SAA control occurs cohesively within the oxide upon its hydration, as evidenced by the high concentrations of O and Al on both sides of the crack. Supporting this conclusion are preliminary XSEM micrographs showing a hydrated corn-flake structure at the crack tip. In contrast, the samples treated with 5000-ppm NTMP, which exhibited poor durability, failed primarily in an adhesive manner, perhaps through the multiple layer of the inhibitor (P was detected on both surfaces.) Here, and presumably with the specimens treated with 500- and 1500-ppm NTMP as well, the inhibitor treatment weakens the polymer-oxide interface with the formation of a hydrogen-bonded inhibitor "film," whose integrity is disrupted by the infusion of water.

On the other hand, the 100-ppm NTMP and Z-6040 treatments appear to have strengthened the oxide-polymer interface. With the Z-6040-treated specimens, crack propagation occurs through both the oxide and adhesive, whereas crack propagation in the 100-ppm NTMP-treated structures occurs entirely within the adhesive. The latter failure mode is more desirable and, in fact, represents the optimum performance of a given adhesive-pretreatment combination, as it shows the weakest link the strength of the polymer.

Based on these data, then, immersion in a 100-ppm aqueous solution of NTMP appears to give the best performance with regard to 1) protection from the environment and 2) promotion of adhesion between the SAA surface and an epoxy system.



## VI. CONCLUSIONS AND RECOMMENDATIONS

The SAA oxide used in this study is porous  $\text{Al}_2\text{O}_3$ , 9- $\mu\text{m}$  thick with an average density (including pores) of ~ 50% that of a dense  $\text{Al}_2\text{O}_3$  thin film. The oxide has the equivalent of approximately one molecular layer of  $\text{Al}_2(\text{SO}_4)_3$  on its surface. Hydration results in a boehmite film that fills the mud cracks and pores of the original oxide. This "sealing" can provide increased corrosion protection for unpainted SAA surfaces, but can lead to problems with bonds to polymer films, due to the moisture-induced volume and morphological changes.

Curing kinetics of the epoxy primer system were found to be first order with times ranging from less than one hour (at 75°C) to more than ten hours (at 27°C). Several of the candidate inhibitors were found to be soluble in the B component, providing a facile means of introducing these compounds into the primer system. The epoxy curing process was not effected in these cases.

The salt-fog corrosion and wedge test experiments were not severe enough to evaluate adequately the relative effectiveness of the inhibitors on SAA surfaces. However, wedge test durability results indicated that a monolayer of NTMP inhibited hydration of the oxide and forced crack propagation into the adhesive -- the failure mode representing the optimum performance of any given adhesive-adherend system.

The NTMP coverage was shown to depend on the solution concentration and pH, with the desired monolayer coverage being achieved from solutions of 10- to 100- ppm NTMP at pH values greater than ~ 3.5.

The results from our work this year demonstrate the need for an improved method to evaluate efficiently the of candidate inhibitors. As a result, three modifications were considered: (1) an accelerated salt-fog process, (2) production of a thinner anodized oxide layer, and (3) use of a non-anodizing surface preparation, such as the FPL etch treatment. After our consultation with NADC personnel, the FPL procedure was chosen to allow for the reliable screening of a wide range of inhibitor compounds. These surfaces have been investigated extensively at the Laboratories, and are not unlike surfaces repaired by protective formulations such as "Pasagel". Inhibitors selected from these tests will ultimately be evaluated, as a pretreatment or repair application, using SAA surfaces exposed to actual environmental conditions.

## VII. REFERENCES

1. H.W. Eicinner and W.E. Schowalter, Forest Products Laboratory, Madison, WI, Report No. 1813 (1950).
2. G.S. Kabayashi and D.J. Donnelly, Boeing Co., Seattle, WA, Report No. DG-41517 (Feb, 1974).
3. Fokker - VFW, Amsterdam, Process Specification TH 6.785 (August, 1978).
4. W.M. McCracken and R.E. Sanders, SAMPE J. 5, 37 (1969).
5. J.C. McMillan, J.T. Quinlivan and R.A. Davis, SAMPE 7, 13 (1976).
6. A.J. Kinloch, ed., Durability of Structural Adhesives, (Applied Science Publishers Ltd., Essex, 1983).
7. P.F.A. Bijlmer and R.J. Schliekeman, SAMPE 5, 13 (1973).
8. A. Pattnaik and J.D. Meakin, Franklin Institute Research Laboratory, Philadelphia, PA, Technical Report 4699 (1974).
9. T. Smith, Rockwell International, Thousand Oaks, CA. Report AFML-TR-74-73 (1975).
10. J.M. Chen, T.S. Sun, J.D. Venables and R. Hopping, Proc. 22nd National SAMPE Symposium, 25 (April 1977).
11. J.D. Venables, D.K. McNamara, J.M. Chen and T.S. Sun, Appl. Surf. Sci. 3, 88 (1979).
12. W. Brockman in Adhesion Aspects of Polymeric Coatings, K.L. Mittal, ed., 265 (Plenum, New York, 1983).
13. J.D. Venables, D.K. McNamara, J.M. Chen, B.M. Ditchek, T.I. Morgenthaler T.S. Sun and R.L. Hopping, Proc. 12th Nat. SAMPE Symposium, Seattle, 909 (October 1980).
14. G.D. Davis and J.D. Venables in Durability of Structural Adhesives, A.J. Kinloch, ed., 43 (Applied Science, Essex, 1983).
15. D.A. Hardwick, J.S. Ahearn and J.D. Venables, J. Mater. Sci. 19, 223 (1984).
16. J.S. Ahearn, G.D. Davis, T.S. Sun and J.D. Venables in Adhesion Aspects of Polymeric Coatings, K.L. Mittal, ed., 281 (Plenum, New York, 1983).
17. J.D. Venables, M.E. Tadros and B.M. Ditchek, U.S. Pat. 4,308,079.
18. D.A. Hardwick, J.S. Ahearn and J.D. Venables (to be published).

19. G.D. Davis, J.S. Ahearn, L.J. Matienzo and J.D. Venables (accepted by J. Mater. Sci.).
20. T.S. Sun, Martin Marietta Laboratories, Baltimore, MD (unpublished results).
21. G.C. Wood, Trans. Inst. Met. Finish 36, 220 (1959).
22. G.E. Thompson, R.C. Farneaux and G.C. Wood, Corros. Sci. 18, 481 (1978).
23. D.J. Arrowsmith and A.W. Clifford, Int. J. Adhes. Adhes. 3, 193 (1983).
24. J.S. Ahearn, T.S. Sun, C. Froede, J.D. Venables and R.L. Hopping, SAMPE Q. 12, 39 (1980).
25. T.S. Sun, D.K. McNamara, J.S. Ahearn, J.M. Chen, B.M. Ditchek and J.D. Venables, Appl. Surf. Sci. 5, 406 (1980).
26. G.D. Davis, T.S. Sun, J.S. Ahearn and J.D. Venables, J. Mater. Sci. 17, 1807 (1982).
27. G.D. Davis, J.S. Ahearn and J.D. Venables, Proc. 15th Nat. SAMPE Tech. Conf., Cincinnati 202 (October 1983).
28. G.D. Davis, J.S. Ahearn and J.D. Venables, J. Vac. Sci. Technol. A 2, 763 (1984).
29. D.K. McNamara, M.S. Thesis, The Johns Hopkins University (1982).
30. G.D. Davis, S. Buchner, W.A. Beck and N.E. Byer, Appl. Surf. Sci. 15, 238 (1983).
31. R.P. Carter, R.L. Carroll and R.R. Irani, Inorg. Chem. 6, 939 (1967).
32. L.V. Nikitina, A.I. Grigorev and N.M. Dyatlova, J. Gen. Chem. USSR, (Engl. Transl.) 44, No.7, 1568 (1974).
33. H.H. Hendrickson, Anal. Chem. 39, 998 (1967).
34. D.A. Hardwick, J.S. Ahearn and J.D. Venables, MML TR 82-23c, End-of-Second-Year Report under Contract N00014-80-C-0718, Martin Marietta Laboratories, Baltimore, MD.
35. G.D. Davis, J.S. Ahearn and J.D. Venables, MML TR 83-34c, End-of-Third-Year Report under Contract N00014-80-C-1718, Martin Marietta Laboratories, Baltimore, MD.
36. K. Wefers, Aluminum 49, 553 (1973).

37. W.J. Bernard and J.J. Randall, Jr., J. Electrochem, Soc. 108, 822 (1961).
38. B.R. Baker, J.D. Balser, R.M. Pearson and E.O. Strahl, Aluminum 52, 241 (1976).
39. D.K. McNamara, Martin Marietta Laboratories, Baltimore, MD (personal communication).